HHS Public Access

Author manuscript

Nat Biotechnol. Author manuscript; available in PMC 2024 July 17.

Published in final edited form as:

Nat Biotechnol. 2024 July ; 42(7): 1065–1074. doi:10.1038/s41587-023-01928-z.

Detecting organelle-specific activity of potassium channels with a DNA nanodevice

Palapuravan Anees[1,2,3], **Anand Saminathan**[1,2], **Ezekiel R. Rozmus**[4], **Anke Di**[5], **Asrar B. Malik**[5], **Brian P. Delisle**[4,*], **Yamuna Krishnan**[1,2,3,*]

[1]Department of Chemistry, The University of Chicago, Chicago, Illinois 60637, USA

[2]Grossman Institute of Neuroscience, Quantitative Biology and Human Behavior, The University of Chicago, Chicago, Illinois 60637, USA

[3]Institute of Biophysical Dynamics, The University of Chicago; Chicago, Illinois 60637, USA

[4]Department of Physiology, University of Kentucky College of Medicine, Lexington, KY, USA

[5]Department of Pharmacology and Regenerative Medicine, The University of Illinois College of Medicine, Chicago, IL 60612

Abstract

Cell surface potassium ion (K^+) channels regulate nutrient transport, cell migration and intercellular communication by controlling K^+ permeability and are thought to be active only at the plasma membrane. Although these channels transit the trans-Golgi network, early and recycling endosomes, whether they are active in these organelles is unknown. Here, we describe a pH correctable, ratiometric reporter for K^+ called *pHlicKer*, use it to probe the compartment-specific activity of a prototypical voltage-gated K^+ channel, Kv11.1, and show that this cell surface channel is active in organelles. Lumenal K^+ in organelles increased in cells expressing wild-type Kv11.1 channels but not when cells were treated with current blockers. Mutant Kv11.1 channels, with impaired cell surface transport, do not increase K^+ levels in recycling endosomes, an effect rescued by pharmacological correction. By providing a way to map the organelle-specific activity of K^+ channels, *pHlicKer* technology could help identify new organellar K^+ channels or channel modulators with nuanced functions.

Cell surface K^+ channels are assembled in the endoplasmic reticulum (ER) and trafficked to the plasma membrane via organelles[1]. The trans-Golgi network (TGN) exports fully

[*]**Correspondence and requests for materials should be addressed to BPD and YK.** brian.delisle@uky.edu, yamuna@uchicago.edu.

Author Contributions

P.A., A.S., and Y.K. designed the sensor and experiments related to its validation. P.A. designed and synthesized the TAC-Rh dye. P.A., B.D and Y.K. designed experiments related to Kv11.1 channels. E.R. performed electrophysiology. P.A. performed all other experiments. P.A. and E.R. analyzed data. A.D. and A.B.M. provided TWIK2 KO BMDM cells. P.A., B.D., and Y.K. wrote the paper. All authors provided input on the manuscript.

Competing financial interests

Y.K. is co-founder of Esya Inc and MacroLogic Inc that use DNA nanodevices for diagnostics and therapeutics, respectively. All other authors declare no competing financial interests.

Supplementary information

Synthetic schemes 1-3, SI Figures 1-15, SI notes 1-4 and SI tables 1-2 are included in Supplementary Information file.

competent K^+ channels to the plasma membrane while early endosomes (EE) sort and deliver endocytosed K^+ channels to recycling endosomes (RE) for return to the plasma membrane. We recently showed these organelles have membrane potentials that could gate various ion channels[2], raising the possibility that cell surface K^+ channels are active in organelles. G-protein coupled receptors (GPCRs) were also formerly thought to be active only at the plasma membrane. However, a conformation-specific fluorescent reporter of GPCRs revealed that they were also activated in organelles by their ligands[3]. Though K^+ channels adopt well-defined activated and inactivated states[4], conformation-specific reporters of K^+ channels do not exist. Hence, we tested the hypothesis that the lumenal K^+ level within an organelle can reveal voltage-gated K^+ channel activity in organelles. For example, if cytosolic K^+ levels exceed that within an organelle, K^+ is expected to flow down the concentration gradient across the organelle membrane and elevate lumenal K^+ when an organelle-resident voltage-gated K^+ channel opens. However, until now, there are no fluorescent reporters of K^+ for acidic organelle lumens.

Every fluorescent K^+ probe works by coordinating K^+ through sp^3 N atoms, where the nitrogen lone pair quenches the fluorophore due to photoinduced electron transfer (PeT)[5–7]. Acidic pH mimics K^+ binding as protonation of the lone pair alleviates PeT and turns the probe on, as well as weakens probe affinity (K_d) for K^+. Further, organelle pH is variable and its effect on membrane potential and lumenal K^+ are difficult to predict. Thus, it is non-trivial to deconvolute the contribution of K^+ from the readout of any fluorescent K^+ indicator in organelles. By indirectly measuring trans Golgi network pH, its lumenal K^+ level was imputed to be 107 mM[8]. The only direct measure of K^+ in organelles so far is that of phagosomal K^+ in neutrophils, reported using electron probe X-ray microanalysis to lie between 200-300 mM[9].

We developed a DNA-based pH-correctable, intracellular K^+ reporter, denoted *pHlicKer*, that can simultaneously report organellar pH and K^+ with single-organelle addressability. We built *pHlicKer* using DNA because it is biocompatible, suitable for quantitative imaging and one can integrate multiple functions in precise stoichiometries into a single assembly[10,11,12]. We targeted *pHlicKer* to either early endosomes, recycling endosomes or the trans Golgi network and mapped lumenal K^+ levels in these organelles. Changes in organellar K^+ levels as a function of K^+ channel expression revealed that cell surface K^+ channels are also active in organelles.

Results

The DNA nanodevice *pHlicKer* accurately detects and measures pH and K^+ levels

pHlicKer is a three-way DNA junction comprising four strands (Fig. 1a and Supplementary Table 2): a 25-mer oligonucleotide conjugated to a K^+ indicator at its 5' end (D_K); a 71-mer strand bearing a reference dye (D_A), a 57-mer strand bearing a pH sensing module (D_D) and a strand harbouring an organelle-targeting motif (D_T). The quaternary complex displays a targeting module (T) that engages a distinct, cognate cell surface receptor that traffics the probe to the relevant organelle[13,14].

The K^+ indicator on D_K is TAC-Rh (Fig. 1a), which has a triazacryptand core connected to rhodamine (λ_{ex} = 560 nm; λ_{em} = 580 nm), azide linkers for conjugation and is based on TAC-Red a known K^+ indicator[7] (see Supplementary Schemes 1–3 and Supplementary Note 1 for synthesis and characterization). In the absence of K^+, rhodamine fluorescence is quenched by PeT from the nitrogen on the triazacryptand. K^+ binding impairs PeT, relieves quenching, and turns on rhodamine fluorescence[7] (Extended data Fig. 1a–b). At acidic pH, protonation of the amines in the triazacryptand both relieves PeT and weakens the affinity (K_d) of TAC-Rh for K^+, thus making it non-trivial to extract the contribution of K^+ to the fluorescence readout (Extended data Fig. 1c). However, given the pH of an individual organelle and knowing precisely how K_d changes with pH, a probe like *pHlicKer* allows us to apply a K_d value suited to the acidic pH of each organelle and thereby obtain lumenal K^+ values with single-organelle resolution. This strategy has been used to quantitate Ca^{2+} in acidic organelles[15]. Attaching TAC-Rh on *pHlicKer* did not change its K_d, which was still 52 mM at pH 7.0 and increases with acidity (Extended data Fig. 1d–e).

The reference dye, Alexa Fluor 647, on D_A is positioned to avoid fluorescence resonance energy transfer (FRET) with TAC-Rh on D_K (Fig. 1a). We chose Alexa Fluor 647 (λ_{ex} = 640 nm; λ_{em} = 665 nm) because it has minimal spectral overlap with TAC-Rh and is insensitive to pH, K^+ and other ions (Supplementary Fig. 1). The 1:1 stoichiometry of Alexa Fluor 647 : TAC-Rh on *pHlicKer* corrects for TAC-Rh intensity changes in cells due to varying probe uptake, or its non-uniform distribution. Thus, the ratio of TAC-Rh (orange channel; O) and Alexa Fluor 647 (red channel; R) intensities in *pHlicKer* and its variants are proportional only to pH and K^+. Hybridization of D_A with D_D reconstitutes a known DNA-based, pH-reporter domain, called the *I-switch*[13], which acts as a ratiometric fluorescent pH reporter (Fig. 1a). Acidic pH causes a conformational change in D_D and leads to high FRET between Alexa 488 (donor, D) on D_D with Alexa 647 (acceptor, A) on D_A.

pHlicKer variants differed from each other only by their respective targeting module, T, encoded on D_T (Extended data Fig. 2a–f). *pHlicKer*^{EE} is transported to early endosomes (EE) by scavenger receptor-mediated endocytosis along with specific pulse and chase times[14]. Similarly, *pHlicKer*^{RE} and *pHlicKer*^{TGN} variants each display a different targeting module (T) that engages either the transferrin receptor or furin to target recycling endosomes (RE) or the trans-Golgi network (TGN) respectively[14,16]. All variants were assembled from equimolar amounts of D_A, D_D, D_K and D_T incorporating the corresponding module T, and characterized by gel electrophoresis (Supplementary Figs. 4–5 and Supplementary Note 3).

To evaluate *pHlicKer* responses, we imaged biotinylated *pHlicKer* (*pHlicKer*^{Biotin}) immobilized on streptavidin-coated beads and measured the Alexa 488 donor-to-Alexa 647 acceptor ratio (D/A) over various pH and [K^+] values for the pH response (Extended data Fig. 3). We also measured TAC-Rh (O) to Alexa Fluor 647 (R) ratio (O/R) for the K^+ response. *pHlicKer* reports pH from pH 5.8-7.0 with a fold change in D/A ratio of 8.5 (Fig. 1b). The D/A response is insensitive to K^+ from 0.1-300 mM (Fig. 1b) while O/R values are sensitive to both K^+ and acidic pH (Fig. 1c). At pH 6.8 of REs, *pHlicKer* response to K^+ shows ~3.8-fold change in O/R (Fig. 1c). Mapping O/R fold change in response to other biologically relevant cations shows that *pHlicKer* is specific to K^+ and its cross reactivity

to other ions is negligible (Fig. 1d). Note that experimental errors in the measurements of D, A, O and R intensities are propagated into the D/A and O/R values, which are in turn propagated into the pH, K_d, O/R_{min} and O/R_{max} parameters of the calibration curve. Since calculating error propagation over the entire chemical space is challenging, we experimentally estimated the errors covering a range of conditions relevant to our study by a blind test (Table S1 and Supplementary Note 4).

Intracellular calibration demonstrates responsiveness of *pHlicKer* to endosomal pH and K^+

We targeted *pHlicKer*^{RE} into REs of HEK 293T cells via transferrin receptors[2] and clamped their lumenal pH and [K^+] using buffers of desired pH and [K^+] containing a cocktail of ionophores (Methods). pH values of the clamping buffer were based on previous estimates of pH in REs, EEs and the TGN while the clamped [K^+] were our projected estimates of extremes that may be encountered in these organelles. Cells were imaged in four channels: (1) Alexa Fluor 488 donor (D) channel; (2) FRET acceptor (A) channel corresponding to Alexa Fluor 647 intensity upon exciting Alexa Fluor 488; (3) TAC-Rh orange (O) channel; and (4) Alexa Fluor 647 red (R) channel (Fig. 2a–d). By taking the ratio of the D image to the A image, we obtain a D/A image that represents the pH map of REs at the clamped pH and K^+ values (Fig. 2e). Similarly, the O/R image represents the K^+ map at the clamped values (Fig. 2f). Representative O/R images clamped at pH 6.6 show that *pHlicKer* responds to high (140 mM; Fig. 2e-f) and low (0.1 mM; Fig. 2g-h) [K^+]. Representative O/R images at pH 6.3 show a weaker response to [K^+] at acidic pH (Fig. 2e-f and Fig. 2i-j). The distribution of D/A versus O/R values confirms this (Figs. 2k–p and Supplementary Fig. S8).

The response characteristics in cells of both the pH and K^+-sensing modules in *pHlicKer* matched the *in vitro* performance. The fold change in D/A ($FC_{D/A}$) values in single endosomes clamped at pH 6.0 and 6.6 quantifies the response of the pH sensing module (Supplementary Fig. S9a) while the fold change in O/R ($FC_{O/R}$) of endosomes clamped at 0.1 mM and 140 mM [K^+] (Supplementary Fig. S9b), and the K_d (Supplementary Fig. S9c) quantify the response of the K^+ sensing module. O/R values of REs clamped at various [K^+] reveals a K_d of 55 mM K^+ at pH 6.6 (Supplementary Fig. S9d). Matching $FC_{D/A}$, $FC_{O/R}$ and K_d values *in cellulo* and *in vitro* indicates the *in vitro* performance characteristics of *pHlicKer* are quantitatively recapitulated in cells.

To obtain absolute [K^+] in EEs, REs, and the TGN in HEK 293T cells, our workflow uses a K_d correction factor at each pixel specified by the pH at that pixel (Fig. 2q–u). As an example, we transformed the D/A map of REs labeled with *pHlicKer*^{RE} into a pH map using the *in cellulo* pH response profile in Supplementary Fig. S9a. The pH map is further transformed into a K_d map by replacing each pixel in the pH map with K_d of *pHlicKer*^{RE} for K^+ at that pH (Methods, Supplementary Fig. S9c). The K_d values for K^+ at each pH is obtained from the *in cellulo* and *in vitro* K^+ response characteristics (Supplementary Fig. S9b–d). The product of the equation $(O/R - O/R_{min})/(O/R_{max} - O/R)$, obtained from the O/R map (Fig. 2t), with the K_d map (Fig. 2s) finally yields the [K^+] map (Fig. 2u). Here, O/R is the observed O/R value at a given pixel in the O/R map, and O/R_{min} and O/R_{max} correspond to the values at 0.1 mM and 140 mM K^+ at the pH value corresponding to the pixel of

interest. [K^+] in EE and TGN can be similarly obtained by labeling them with *pHlicKer*^{EE} and *pHlicKer*^{TGN}, respectively.

pHlicKer maps pH and K^+ in endocytic organelles.

Because cell surface K^+ channels transiting REs, EEs as well as the TGN are fully glycosylated and destined for plasma membrane insertion, we used *pHlicKer* to test whether channels are active in these organelles. To test channel activity, we must first know the resting K^+ levels in these organelles so that we may predict the direction of K^+ flow should the channels open. We began by localizing *pHlicKer*^{EE}, *pHlicKer*^{TGN}, and *pHlicKer*^{RE} variants in EE, TGN and RE of HEK 293T cells, respectively (Fig. 3a). We used HEK 293T cells because they have low endogenous expression of voltage-gated K^+ channels[17]. For evaluating targeting specificity, the corresponding *pHlicKer* variants carrying only the Alexa Fluor 647 reference dye (3W^{EE}, 3W^{TGN}, 3W^{RE}) were used (Fig. 3a and Extended data Fig. 2d–f). Because HEK 293T cells do not express scavenger receptors[18,19,20,21,22] required for endocytosis of 3W^{EE} or *pHlicKer*^{EE}, we transiently transfected the cells with human macrophage scavenger receptor (hMSR1)[2] (Extended data Fig. 4a–b). Using previously demonstrated strategies, *pHlicKer*^{RE} targets the human transferrin receptor (TfR) using an RNA aptamer against TfR[2,16]. Similarly *pHlicKer*^{TGN} binds a single-chain variable fragment recombinant antibody, scFv, fused to the extracellular domain of furin, via a $d(AT)_4$ sequence[2,14].

Time-dependent colocalization experiments between 3W^{EE} and an endocytic tracer such as Alexa 488-labeled transferrin (Tf-A488) revealed that a 10 min pulse of 3W^{EE} led to 70±0.5% colocalization in EEs (Fig. 3b). Similarly, 3W^{RE} showed 78±0.7% colocalization in REs of HEK293T cells (Fig. 3c). Excess unlabeled transferrin (Tf) competed out the uptake of 3W^{RE}, confirming that *pHlicKer*^{RE} was internalized via the TfR pathway (Extended data Fig. 4c–d). Pulsing and chasing 3W^{TGN} for 90 min each traffics the former to the TGN as seen from 85±0.4% colocalization with TGN46-mCherry (Fig. 3d). Based on these results, we delivered *pHlicKer*^{RE} to REs and measured their lumenal pH and [K^+]. From the D/A and O/R images, we computed the pH and [K^+] of ~100 REs as described in Fig. 2q–u. The pH value of an RE versus its corresponding [K^+] for ~100 REs yields a scatter plot (Fig. 3e), which we converted into a colour-coded, density plot for clearer visualization, referred to hereafter as a two-ion measurement (2-IM) plot[22] (Fig. 3f). Similar 2-IM plots for EEs and TGNs were constructed from their respective D/A and O/R images (Figs. 3g-i). Consistent with earlier reports[14,23], the 2-IM plots show the pH of REs, EEs, and TGN centered at pH 6.5±0.1, 6.1±0.01 and 6.3±0.01, respectively. The lumenal [K^+] was centered at 40±1 mM for REs, 19±1 mM for EEs and 102±3 mM for TGN (Fig. 3f, h, i). K^+ levels obtained with *pHlicKer*^{TGN} are consistent with the previous indirect measure in the TGN using null point titration.[8] Notably, the high transmembrane [K^+] gradient across EEs implies that K^+ flux contributes substantially to EE membrane potential while the much lower gradient across the TGN suggests that other ions may be bigger contributors to TGN membrane potential[5]. Just as the activity of organelle-resident Cl^- channels and transporters alters lumenal Cl^- levels in organelles[16,24], we predict that K^+ channel activity in EEs, REs and the TGN will elevate lumenal K^+ since K^+ levels in all three organelles are lower than the cytosol.

pHlicKer reveals K^+-channel activity in the recycling endosome and trans-Golgi Network

Next, we tested whether the activity of a K^+ channel in organelles could increase its lumenal K^+ levels in a physiological system. The functionality of the two pore K^+ channel, TWIK2 on the cell surface of macrophages is critical for inflammation.[25] Recently TWIK-2 was found to also reside in REs, yet its activity in these compartments has not been tested.[26] We could efficiently label REs in bone marrow derived macrophages (BMDMs) with *pHlicKer*^{RE} with a 15 minute pulse and 30 min chase (Fig. 4a,b). The K^+ levels in REs of wild-type BMDMs was 52±1 mM, which dropped to 23±1 mM in those from a TWIK-2 KO mouse. Thus the presence of TWIK-2 in REs elevates the lumenal K^+ levels suggesting this channel opens in RE membranes (Fig. 4c–e). Despite the ~20 mM drop in K^+, the lumenal pH changed negligibly (~40 nM). This suggests that lumenal pH in REs is set by factors other than K-channels that compensate for K^+ influx due to K-channel activity.

Next, we used *pHlicKer* to measure the activity, if any, of a canonical cell-surface, voltage-gated K^+ channel such as the *KCNH2*-encoded Kv11.1 channel in the TGN and in REs. Kv11.1 channels represent an ideal test case because they are formed by tetramerization of the prototypical pore-forming voltage-gated K^+ channel subunits and their activity is critical for normal cardiac excitability[27–29]. Nearly 90% of the ~200 *KCNH2* missense mutations are linked to the deadly pro-arrhythmic long QT syndrome (LQTS)[30–31]. Defective trafficking of selected mutant Kv11.1 channels can be corrected in cells by incubating them with drugs that bind Kv11.1 channels[30]. We studied the activity in TGN and REs because Kv11.1 trafficking can be monitored biochemically[31]. The TGN has high membrane potential, suggesting vigorous ion transport[5]. Further, if Kv11.1 channels are produced and secreted successfully, the TGN lies early on their transport pathway. REs double as storage compartments for cell surface ion channels, after plasma membrane insertion, endocytosis and sorting[32,33]. Functional Kv11.1 channels reach these organelles later. Because HEK 293T cells do not endogenously express Kv11.1 channels, we stably expressed wild type Kv11.1 channels in these cells (WT cells)[17] (Fig. 5a). Coimmunostaining experiments showed that Kv11.1 is present in the TGN and RE of WT cells (Supplementary Fig. S11 and S12).

First, we tested whether endogenously expressed K^+ channels were active in the TGN given their high resting K^+ levels. Hence, we treated cells with a pan voltage-gated K^+ channel current inhibitor, i.e., tetraethyl ammonium chloride (TEA). Although TEA is membrane-impermeable, we reasoned that, at 10 mM, enough might accumulate in organelle lumens due to sustained rounds of fluid phase endocytosis which could potentially inhibit the organellar fraction of Kv11.1. Notably, K^+ levels in the TGN ($[K^+]_{TGN}$) decreased significantly to 73±4 mM (Fig 5b–c and 5f–g), indicating the functionality of TGN-resident K^+ channels. This is consistent with its high membrane potential, which indicates ample ion transport across these membranes. When we measured $[K^+]_{TGN}$ in cells expressing WT Kv11.1 channels we found that $[K^+]_{TGN}$ was significantly elevated to 117±5 mM (Fig. 5d,h and Supplementary Fig. S14). However, treatment with cisapride, a highly specific inhibitor of Kv11.1 channel current ($I_{Kv11.1}$)[34], reduced $[K^+]_{TGN}$ to 95±4 mM in WT cells but not UT cells (Supplementary Fig. S13). The reduction in $[K^+]_{TGN}$ indicates the specific activity of Kv11.1 channels in the TGN, given their contribution to the lumenal K^+ (Fig. 5e and 5i).

K^+ levels in REs ($[K^+]_{RE}$) of cells expressing WT Kv11.1 was also significant elevated to 78±4 mM (Fig. 3f and 6b) from the 40±1 mM resting levels in HEK 293T cells lacking Kv11.1 channels (UT cells) (Fig. 3f). When WT cells were treated with TEA, $[K^+]_{RE}$ reverted to resting levels of 36 mM±2 mM (Fig. 6b, c). Neither TEA nor cisapride altered $[K^+]_{RE}$ in UT cells (Fig. 6d and Supplementary Fig. S13). When WT cells were treated with cisapride, $[K^+]_{RE}$ levels plunged to 38±2 mM, indicating that the reduced $[K^+]_{RE}$ in WT cells is due to inhibition of $I_{Kv11.1}$ in REs (Fig. 6e). Together, these results indicate that Kv11.1 channels open in REs, and that channel opening changes lumenal $[K^+]$.

Here too, pH_{RE} did not alter appreciably when K^+ levels changed due to channel activity, as we observed in BMDMs. RE and TGN membranes contain organelle-resident pH regulators such as H^+/Cl^- exchangers and Na^+/H^+ exchangers (NHE 9 and NHE-7).[35] NHEs can exchange both K^+ and Na^+ for H^+. Other regulators that may be found on the TGN or RE prior to plasma membrane insertion or due to recycling respectively, are Na^+ channels, Na^+/K^+ ATPase and H^+/K^+ ATPase.[36,37] These players could jointly maintain luminal pH despite the influx of K^+, just as when a cell-surface K-channel opens, even though the membrane potential and cytosolic K^+ change, the cytosolic pH does not.

pHlicKer tracks channel activity and trafficking

pHlicKer can also reveal the presence of an active K^+ channel in an endocytic organelle. We stably expressed Kv11.1 channels with a Gly601Ser missense mutation in HEK 293T cells (G601S cells) and measured the $[K^+]_{RE}$. This mutation, linked to LQTS[31], disrupts protein folding and channel trafficking[38], causing Kv11.1 to be retained in the ER and subsequently degraded (Supplementary Fig. S15). ER retention alters the cell surface abundance of Kv11.1 and affects current density. We found that $[K^+]_{RE}$ levels in G601S cells was 38±3 mM, far below WT cells and commensurate with UT cells. This is consistent with a model where REs lack G601S-Kv11.1 channels, as they are retained in the ER, do not reach the cell surface and hence do not enter the recycling pathway (Fig. 6f).

To test whether G601S-Kv11.1 mutant channels can recycle and are active in REs, we cultured G601S cells with dofetilide and measured $[K^+]_{RE}$. Drugs such as dofetilide block $I_{KV11.1}$[30] and act as pharmacological chaperones that facilitate the folding of mutants like G601S-Kv11.1 (Supplementary Fig. S15)[39]. Dofetilide (10 uM) treatment for 8 h allows G601S-Kv11.1 channels to exit the ER, enter the secretory pathway and reach the cell surface[40] (Fig. 6a). We found that after treatment and 1 h wash out of dofetilide restored $[K^+]_{RE}$ to levels that were comparable to WT cells (Fig. 6g), indicating that properly folded G601S-Kv11.1 channels recapitulate the trafficking and activity of WT-Kv11.1 channels even after they reach the cell surface.

Electrophysiological studies at the plasma membrane further confirm that WT-Kv11.1 channels are active under conditions that mimic those at the RE membrane (Fig 6h). We used whole-cell voltage-clamp to measure $I_{Kv11.1}$ in WT and G601S cells incubated with standard extracellular saline or a modified saline that recapitulated the transmembrane ion gradients of pH, Na^+, K^+ and membrane potential experienced by the channel in RE membranes. Whole cell $I_{Kv11.1}$ in standard extracellular saline was recorded using a holding potential of −80 mV. To measure the voltage-dependence of Kv11.1 channel opening, cells

were pre-pulsed from −80 mV to 70 mV in 10 mV increments for 5 s immediately followed by a test pulse to −50 mV for 5 s (Fig. 6i and Extended data Fig. 5a). Because of changes in reversal potential for $I_{Kv11.1}$ and the kinetic changes in Kv11.1 channel deactivation gating, the whole cell $I_{Kv11.1}$ in modified extracellular saline was recorded using a holding potential of −100 mV and cells were pre-pulsed in the same way but were followed by a test pulse to −100 mV for 5 s (Fig. 6j and Extended data Fig. 5b). The peak inward and outward $I_{Kv11.1}$ measured during the test pulse in standard and modified saline, respectively, were plotted as a function of the pre-pulse potential and the corresponding I-V relations were fitted with a Boltzmann function to calculate the I_{MAX} (Fig. 6k–l), $V_{½}$ (Extended data Fig. 5c), and *k* (Extended data Fig. 5d).

In both types of saline, WT cells have larger $I_{Kv11.1}$ than G601S cells (Fig. 6i, j), consistent with G601S-Kv11.1 channels failing to reach the cell surface. The opening properties of WT- or G601S-Kv11.1 channels in both types of saline are similar. In fact, under conditions mimicking the RE environment, the voltage dependence of Kv11.1 channel opening ($V_{½}$) was slightly negatively shifted (Extended data Fig. 5c), indicating that some channels are open at the ionic conditions and membrane potentials experienced in REs.

Discussion

Organelle-targeted DNA nanodevices that act as pH correctable, ratiometric K^+ reporters can address the compartment-specific activity of a cell surface K^+ channel. Here, by applying *pHlicKer*, we could demonstrate that cell surface K^+ channels are active in organelles unlike thought previously. *pHlicKer* technology combines a pH and K^+ reporter on a single DNA scaffold, provides information on both ions with single-organelle addressability, and thereby allowed us to test a long-standing tenet that the organelle-resident fraction of cell surface K^+ channels are inactive.

Unlike small molecules or protein-based fluorescent K^+ reporters, which are pH sensitive and have only been used at neutral pH in the cytoplasm or nucleus[41], *pHlicKer* allows us to introduce an organelle-specific pH-correction factor that in turn allows us to extract the contribution of K^+ in acidic organelles. *pHlicKer* revealed that resting K^+ levels in EE, REs and the TGN were lower than cytosolic levels and indicated that channel activity in the membrane of these organelles would elevate lumenal K^+. Currently, *pHlicKer* cannot be applied to endolysosomes, for two-photon or real-time imaging due to limitations of the K^+ sensitive dye TAC-red. These limitations may be potentially overcome by engineering either less pH-sensitive, more photostable or two-photon active analogues of the K^+ sensitive dye TAC-red to yield *pHlicKer* variants suited to study endolysosomes, or real-time imaging of K^+ fluxes or *in vivo* K^+ imaging.

By using the first generation of *pHlicKer* variants to study the TGN and REs, we discovered that K^+ channel activity in organelles did indeed increase lumenal K^+ levels as ions flowed down the transmembrane gradient. Cells with blocked Kv11.1 channel activity or those expressing trafficking-defective G601S-Kv11.1 mutant channels, showed lower K^+ levels in REs than those with functional WT Kv11.1 channels. When trafficking was restored with dofetilide, lumenal K^+ reverted to levels commensurate with REs harbouring WT Kv11.1

channels. We confirmed channel opening by electrophysiology at the plasma membrane using ionic conditions and membrane potentials that mimic those across the RE membrane.

For voltage-gated ion channels to become active, the membrane potential must change dramatically and rapidly.[42] We previously reported the membrane potential distributions of an ensemble of REs and TGNs across ~10 cells captured at a single timepoint.[2] The spread suggests that, for example, while an RE is most often found to exist at −70 mV it can sample a range of membrane potentials. Thus, one can envisage that if some event depolarizes the organelle membrane, this may lead to a K^+ channel opening and repolarizing the membrane, thereby allowing the organelle to restore its membrane potential. Such membrane depolarization may likely involve an organelle-resident or endosomally-localized cell-surface Na^+ channel.

Cell surface channels such as Kv11.1 were previously considered to be inactive in organelles because their activity is facilitated by PIP2, which is abundant in the plasma membrane, but not in organelles.[43–44] Since Kv11.1 channels show activity in organelles, it is interesting to consider how such activation might occur. Other phosphoinositides present on RE and TGN membranes might activate channels. Alternatively, RE membranes and vesicles from the TGN have been shown to have small quantities of PI(4,5)P2 that may suffice to activate channels. Particularly in the RE and TGN, PI(4,5)P2 existence and functionality is supported by the presence of PIP Kinases and PI(4,5)P2 effectors such as PIPK1, AP1B, EHD-1 SNX18, syntenin and SNX9.[45] The non-responsivity of organellar PI(4,5P)2 to detection by immunofluorescence has been ascribed to these limited amounts being bound to so many effectors in organelles, that very little is free for detection.[45]

Our findings suggest that the activity of cell-surface K^+ channels in organelles could have distinct functional consequences and hence, wider roles than previously thought. Such K^+ channel activity could contribute to organelle membrane potential and hence, its latent ability to regulate intracellular trafficking. The acidic lumenal pH and different membrane potential of the organelle will affect the open/closed probabilities of the channel. In turn, the new residence time of the channel in the closed (or open) state, could regulate when an endosome matures to next the stage. Thus, the residence times of a K^+ channel in the open or closed states could form the heart of an “endocytic clock”. Channel opening/closing could similarly act as an exocytic clock since organelle pH also decreases along the secretory pathway.

More broadly, because *pHlicKer* technology offers a practical route to map organellar K^+ changes due to K^+ channel activity, it can be adapted to study the compartment-specific activity of other cell surface channels, or organelle-resident K^+ channels at a higher level of cellular detail.[46,47] *pHlicKer* can also be deployed to discover new organelle-resident K^+ channels and transporters, identify organelle-selective modulators of K^+ channel activity, and understand the mechanisms that modulate cell-surface K^+ channel abundance.

Methods

Reagents.

All oligonucleotides (Supplementary Table 2) used in this study were purified by high performance liquid chromatography (HPLC) and purchased from Integrated DNA Technologies (USA). All oligonucleotides were subjected to ethanol precipitation and quantified using UV absorbance. ^{1}H NMR and ^{13}C NMR spectra of the newly synthesized compounds were recorded on a Bruker AVANCE II+, 500 MHz NMR spectrophotometer in $CDCl_3$ and tetramethylsilane (TMS) was used as an internal standard. Mass spectra were recorded with an Agilent 6224 Accurate-Mass time-of-flight (TOF) liquid chromatography–mass spectrometry (LC/MS). Streptavidin-coated microspheres were purchased from Bangs Laboratories, Inc. Maleylated BSA (mBSA) and fluorescent transferrin (Tf-Alexa488) were synthesized according to previously published protocols[13,16,48]. Valinomycin, nigericin, and monensin were purchased from Cayman Chemicals. All other reagents were purchased from Sigma-Aldrich (USA) unless otherwise specified.

TAC-Rh conjugation and sample preparation.

TAC-Rh-N_3 was conjugated to D_K. TAC-Rh-N3 (25 μM) was added to 5 μM DBCO labeled D_K in 100 μL of sodium phosphate (10 mM) buffer containing KCl (100 mM) at pH 7.0. The reaction was stirred overnight at room temperature to achieve a 1:1 labeling of ssDNA with the TAC-Rh-N3. The reaction mixture was ethanol precipitated multiple times (12000 rpm for 10 min at 4 °C) to remove unreacted TAC-Rh-N3[2]. A ratio of 1:1 labeling of the TAC-Rh to the DNA was confirmed by using UV-Vis spectroscopy (Supplementary Fig. S2). See Supplementary Fig. S4A for gel characterization of the product.

Construction of *pHlicKer*^{Biotin}, *pHlicKer*^{RE}, *pHlicKer*$^{EE/TGN}$.

Stock solution of *pHlicKer* derivatives were prepared at a final concentration of 10 μM by mixing D_K (K^+ sensing strand), D_D (Atto488N strand), D_A (Atto647N strand) and D_T (targeting moiety modified strand) in an equimolar ratio in 20 mM sodium phosphate buffer, pH 5.5, containing 100 mM KCl (Supplementary Figs. 4–7). For all samples, annealing and gel characterization were performed according to a previously established protocol[2]. Gels were run in 1 × TBE buffer (100 mM Tris·HCl, 89 mM boric acid, and 2 mM EDTA, pH 8.3) at RT. Gels were observed under a Biorad Universal Hood II Gel Doc System (Bio-Rad Laboratories, Inc.) using Image Lab Software 6.0.0 for image acquisition for Alexa488, TMR and Alexa 647 channels. After measurement, gels were stained with ethidium bromide (1 μ g ml^{-1}) and observed.

In vitro spectroscopic measurements.

Fluorescence spectra were recorded on a FluoroMax-4 scanning spectro-fluorometer (Horiba Scientific, Edison, NJ, USA) using previously established protocols.[13] For recording the spectra, *pHlicKer* Samples were diluted to 200 nM in UB4 buffer (20 mM HEPES, MES and sodium acetate, 140 mM NaCl/KCl, 1 mM $CaCl_2$ and $MgCl_2$) of the desired pH and K^+ concentrations was excited at 495 nm, 560 nm and 640 nm, and the emission spectra were collected at 515–750 nm, 570–620 and 650–750 nm, respectively (Extended Data Fig. 1).

Cell culture, plasmids and transfection.

Human embryonic kidney cells (HEK 293T) cells were gifts from B. Dickinson (University of Chicago). Cell line was checked for mycoplasma contamination using Hoechst-33342 staining. Cells were cultured in Dulbecco's Modified Eagle's Medium (Invitrogen Corporation, USA) containing 10% heat-inactivated fetal bovine serum (FBS) (Invitrogen Corporation, USA), 100 Uml^{-1} penicillin and 100 μg/ml streptomycin, and maintained at 37 °C under 5% CO2. HEK 293T cells were passaged and plated at a confluency of 50-70% for transfection and intracellular measurements. Both hMSR1 and scFv-furin constructs are reported previously[2,14]. HEK 293T cells were transiently transfected with the respective plasmids using TransIT-293 transfection reagent (MIRUS). After incubation for 4 h, the transfected medium was replaced with fresh medium. Cells were labelled 48 h post transfection. Human embryonic kidney 293 (HEK293) cell lines expressing wild-type Kv11.1 (WT) or the trafficking-deficient G601S-Kv11.1 channel proteins are described previously[49]. Cells were cultured at 37 °C (5% CO_2) in MEM supplemented with 10% fetal bovine serum (Invitrogen) and geneticin.

Competition experiments. Scavenger receptor mediated endocytosis of $3W^{EE}$.

HEK 293T cells transfected with hMSR1 were incubated with 20 μM mBSA or BSA for 15 min and pulsed with a media containing 500 nM $3W^{EE}$ and 20 μM of mBSA or BSA for 1 h at 37 °C. Cells were washed with 1× PBS three times and then imaged. Whole-cell intensities of 15 cells per dish in the A647 channel were quantified.

Transferrin receptor mediated endocytosis of $3W^{RE}$.

Two different dishes containing HEK 293T cells were prepared. The first dish was incubated with 20 μM of free Tf for 10 min at 37 °C. Then the cells were pulsed with a mixture of 500 nM $3W^{RE}$ and 20 μM of free Tf for 30 min at 37 °C. The second dish was pulsed with 500 nM $3W^{RE}$ alone (-free Tf) for 30 min at 37 °C. Both the cells were then chased for 30 min. Cells were washed with 1× PBS three times and then imaged. Whole-cell intensities of 15 cells per dish in the A647 channel were quantified.

Co-localization and labelling experiments.

Co-localization experiments were performed by following the previously reported protocols.[2] Fluorescent transferrin (Tf-A_{488}) was used to specifically label EE by pulsing it for 10 min prior to imaging and to label RE with an additional chase time of 30 min[50]. Transient expression of TGN46-mCherry specifically labels the trans-Golgi network (TGN)[51]. Time required for the delivery of DNA devices with a transferrin aptamer and d(AT)4 tag when labelling RE and TGN, respectively, has been determined previously[16,14,52]. Briefly, recycling endosomes are targeted by pulsing HEK 293T cells and BMDM cells with 100 nM Tf-A_{488} and 500 nM $3W^{RE}$ in Hank's Balanced Salt Solution (HBSS) for 15 minutes, followed by 30 min of chase in complete media at 37 °C. To label EE, HEK 293T cells transiently transfected with hMSR1, were pulsed with 100 nM Tf-A_{488} and 500 nM $3W^{EE}$ for 10 minutes and chased for 10 min. The trans-Golgi network is targeted by pulsing $3W^{TGN}$ to scFv-furin-transfected HEK 293T cells for 90 min, followed by 90 min chase. Crosstalk and bleed- through were recorded and discovered

to be negligible between the A647 channel and organelle markers. Pearson's correlation coefficient (PCC) measures the pixel-by-pixel covariance of two images while it ranges from 0-1, and 1 indicates complete colocalization. PCCs are examined by the tool in ImageJ/Fiji 2.0.0-rc-54/1.51 h. On pixel shift, PCC values decrease significantly suggesting non-random colocalization.

Confocal imaging.

Confocal images were captured with a Leica TCS SP5 II STED laser scanning confocal microscope (Leica Microsystems, Buffalo Grove, IL, USA) equipped with a ×63, 1.4 NA, oil immersion objective. Alexa Fluor 647 was excited using a He–Ne laser with a wavelength of 633 nm and recorded using hybrid detector (HyD).

In vitro bead calibration of *pHlicKer.*

Bead calibration was performed using $pHlicKer^{Biotin}$ labelled 1-μm streptavidin coated microspheres (Bangs Laboratories, Inc.). Briefly, streptavidin coated microspheres were incubated in a solution of 5 μM $pHlicKer^{Biotin}$ in 20 mM sodium phosphate buffer, pH 5.5 and 140 mM NaCl and left for gentle mixing at room temperature. After 2 hours of shaking, the beads were collected by centrifuging at 5,000 rpm and stored in pH 5.5 and 150 mM NaCl. 0.05% of Tween-20 was added to prevent aggregation of beads. This binding solution was then spun down and the beads were reconstituted in clamping buffer (HEPES (20 mM), MES (20 mM), sodium acetate (20 mM), $CaCl_2$ (1 mM), $MgCl_2$ (1 mM), solutions were balanced with NaCl to maintain a constant ionic strength of 140 mM) with varying conc. of $[K^+]$ and pH. The bead solution was then drop casted on an imaging dish with cover slip and incubated for 30 min at 37 ℃. After 30 min incubation, beads were imaged on the IX83 inverted microscope.

Fluorescence imaging of beads.

Bead imaging was done using IX83 inverted wide field microscope (Olympus Corporation of the Americas, Center Valley, PA, USA) using either a ×100 or ×60, 1.42 numerical aperture (NA), differential interference contrast (DIC) oil immersion objective (PLAPON) and Evolve Delta 512 EMCCD camera (Photometrics, USA), and controlled using MetaMorph Premier Ver 7.8.12.0 (Molecular Devices, LLC, USA), suitable for the fluorophores used. Alexa Fluor 488 channel images (D) were obtained using a 480/20 band-pass excitation filter, a 520/40 band-pass emission filter, and an 89016-ET-FITC/Cy3/Cy5 dichroic filter. FRET channel images (A) were obtained using the 480/20 band-pass excitation filter, 705/72 band-pass emission filter, and 89016-ET-FITC/Cy3/Cy5 dichroic filter. TAC-Rh channel images (O) were obtained using a 545/25 band-pass excitation filter, a 595/50 band-pass emission filter, and a an 89016-ET-FITC/Cy3/Cy5 dichroic filter. Alexa647N channel images (R) were acquired using 640/30 band pass excitation filter, 705/72 band pass emission filter and 89016 dichroic.

Image analysis of beads.—Images were analyzed using Fiji (NIH, USA). For K^+ and pH measurements, regions around the beads in each Alexa647N (R) image were identified and marked in the ROI plugin in ImageJ. The same regions were identified in the other channels by recalling the ROIs. Similarly, for background computation, a nearby

region outside the beads was manually selected and saved as an ROI. The same regions were selected in the other channels by recalling the ROIs. Then, we measured the mean fluorescence intensity in each bead in donor, acceptor, TAC-Rh (O), and Alexa Fluor 647 (R) channels, and the background intensity corresponding to that image and channel was subtracted. The two ratios of intensities (D/A and O/R) were then computed for each bead.

Calculating pH-corrected [K^+].—The ratio intensities of D and A (D/A) was plotted as a function of pH to generate the pH calibration curve as shown in Supplementary Fig. S10A, which was fitted to a Boltzmann sigmoid equation:

$$\mathrm{pH} = \mathrm{pH}_{1/2} + \ln[((\mathrm{A}_1 - \mathrm{A}_2)/(\mathrm{D/A}) - (\mathrm{A}_2)) - 1] \times 0.1241$$

where A1, A2, and $\mathrm{pH}_{1/2}$ represent parameters from a Boltzmann fit of the pH calibration curve, and Y represents the D/A ratio.

The pH dependence of *pHlicKer*'s K^+ sensing is given by two parameters: K_d of *pHlicKer* and fold-change in O/R given by the ratio of $\mathrm{O/R_{min}}$ to $\mathrm{O/R_{max}}$ at every pH. We measured the K_d at different pH points ranging from 5.5 to 7.0 by fitting an exponential equation to measured K^+ calibration curves as shown in Supplementary Fig. S10B. The K_d of *pHlicKer* was plotted as a function of pH using the following equation:

$$K_d = 46.96 + 548244 \times \mathrm{e}^{-1.627 \times \mathrm{pH}}$$

We obtained $\mathrm{O/R_{min}}$ i.e., the O/R at low [K^+], by clamping beads at 0.1 mM [K^+] at different pH points.

$$\mathrm{O/R}_{min} = 3.18 + \left[\left(-6.01/\left(\left(1.766\right) \times \sqrt{(3.14/2)}\right)\right] \times \left[e\left(-2 \times \left(\left(pH - 6.25\right)/1.766\right)^2\right.\right.\right.$$

$\mathrm{O/R_{max}}$ i.e., the O/R at high [K^+] by clamping beads at 140 mM [K^+] at different pH points.

$$\mathrm{O/R}_{max} = 131.6 - \left(43.66 \times \mathrm{pH}\right) + \left(3.64 \times \mathrm{pH}^2\right)$$

pH and O/R were used to calculate K_d, $\mathrm{O/R_{max}}$ and $\mathrm{O/R_{min}}$ from equations (2)-(4). Finally, K_d, $\mathrm{O/R_{min}}$, O/R, and $\mathrm{O/R_{max}}$ were substituted in the following equation to get pH-corrected free [K^+] values:

$$\left[\mathrm{K}^+\right] = \mathrm{K}_d \times \left[\left(\mathrm{O/R} - \mathrm{O/R}_{mini}\right)/\left(\mathrm{O/R} - \mathrm{O/R}_{max}\right)\right]$$

In cellulo* measurement of pH and [K^+].—In cellulo* clamping: pH and potassium clamping were carried out using *pHlicKer*^{RE} or *pHlicKer*$^{\mathrm{EE/TGN}}$. HEK 293T cells were pulsed with 250 nM *pHlicKer*^{RE} for 15 min and chased for 30 min at 37 °C. Cells were then fixed with 200 μL of 4% paraformaldehyde for 5 min at 25 °C. The fixed cells were washed

with 1 × PBS three times and incubated in the potassium clamping buffer of indicated pH and potassium concentration, containing 50 μM nigericin, 50 μM monensin and 20 μM valinomycin for 1 h at 37 °C. Clamping buffers with various concentration of potassium ions were prepared by adding potassium positive buffer (140 mM KCl, 1 mM $CaCl_2$, 1 mM $MgCl_2$, 20 mM HEPES, MES, sodium acetate) to a K^+ negative buffer (140 mM NaCl, 1 mM $CaCl_2$, 1 mM $MgCl_2$, 20 mM HEPES, MES, sodium acetate) at the same indicated pH in different ratios. The cells were then imaged in clamping buffer using a widefield microscope.

EE and TGN pH and [K^+] measurements were carried out using *pHlicKer*$^{EE/TGN}$ in HEK 293T cells transfected with hMSR1 and scFv-furin respectively. For EEs, HEK 293T cells were pulsed with 250 nM *pHlicKer*^{EE} for 10 min and chased for 10 min. For TGN, HEK 293T cells were pulsed with 250 nM *pHlicKer*^{TGN} for 90 min and chased for 90 min. Cells were washed with 1× PBS three times and then imaged. For recycling endosomes, HEK 293T cells were pulsed with 250 nM *pHlicKer*^{RE} for 15 min and chased for 30 min. Cells were washed with 1× PBS three times and then imaged using a widefield microscope.

Image analysis: Images were analyzed using Fiji (NIH, USA). For organellar K^+ and pH measurements, regions of cells containing single isolated endosomes in each Alexa647N (R) image were identified and marked in the ROI plugin in ImageJ. The same regions were identified in the other channels by recalling the ROIs and appropriate correction factor for chromatic aberration if necessary. Similarly, for background computation, a nearby region outside the endosomes was manually selected and saved as an ROI. The same regions were selected in the other channels by recalling the ROIs. Then, we measured the mean fluorescence intensity in each endosome in D, A, TAC-Rh (O), and Alexa Fluor 647 (R) channels, and the background intensity corresponding to that cell and channel was subtracted. The two ratios of intensities (D/A and O/R) were then computed for each endosome. Mean D/A of each distribution was plotted as a function of pH to obtain the in cellulo pH calibration curve. Mean O/R of each distribution was plotted as a function of [K^+] to generate the in cellulo K^+ calibration curve. Pseudocolor pH and K^+ images were obtained by measuring the D/A and O/R ratios per pixel, respectively.

Calculating pH-corrected [K^+] in early endosomes, trans-Golgi network, and recycling endosomes.

To correct for pH and obtain K^+ values, the K_d of *pHlicKer* in single endosomes was calculated based on the K_d calibration plot versus pH. The pH of the organelle was measured from the D/A values calibrated across pH 5.5-7.0. Donor (D) and acceptor (A) images were background subtracted by drawing a region of interest outside the cells. The D image was duplicated, and a threshold was set to create a binary mask. Background-subtracted D and A images were then multiplied with the binary mask to get processed D and A images. This processed D image was divided by the processed A image to get a pseudocolor D/A image, using the Image Calculator module of ImageJ. The pH value at every pixel was computed by applying equation (1) formulated from an *in vitro* pH calibration plot, using ImageJ.

The pseudocolored pH image was processed to get a K_d image (Supplementary Fig. S9). K_d of *pHlicKer* is a function of pH and this relation is formulated by the K_d calibration plot *in vitro* using equation (2). To convert the pH image to a K_d image, the background was set to a non-zero value. The pH-dependent K_d correction was performed according to equation (5), where O/R_{max} and O/R_{min} were calculated from *in cellulo* clamping at 140 mM and 0.1 mM K^+, respectively. Image calculations were done using the Image Calculator module in ImageJ. This image was multiplied with the binary image to bring the background value to zero.

Immunofluorescence.—Kv11.1 over expressing HEK 293T cells were fixed in 4% PFA in 1X PBS for 15 mins. Cells were permeabilized in 0.25% Triton X 100 for 15 mins, RT. Blocking was performed in 1X PBS containing 3% BSA for 30 min. Cells were then incubated with indicated primary antibodies: rabbit anti-Kv11.1 antibody (Alomone Catalog no. APC-062) (1:500), mouse monoclonal anti-58K antibody (Abcam Catalog no. ab27043) (1:200) or mouse monoclonal Transferrin receptor antibody (Thermofischer Catalog no. 13-6800) (1:200) in blocking buffer (3% BSA in 1X PBS) for 1 h at room temperature. Cells were then washed for 5 min with 1X PBS (3x). After washing, cells were treated with Goat anti-rabbit secondary antibody conjugated with Alexa Fluor 647 (Life Technologies, cat. no. A21244, 1:1,000 dilution) and Goat anti-Mouse secondary antibody conjugated with Alexa-488 (Life Technologies, cat. no. A11001, 1:500 dilution) in PBS containing 3% BSA. Cells were washed and imaged using confocal microscope.

Pharmacological drug treatments.—*pHlicKer* labelled cells were treated with TEA (10 mM) or cisapride (10 μM) for 10 min in HBSS solution at room temperature. Cells were imaged in HBSS containing the respective blocker compounds.

Restoration of trafficking.—To correct trafficking of Kv11.1 channels, HEK 293T cells expressing G601S- Kv11.1 were cultured for 24 h at 37 °C with 10 μM dofetilide and washed with PBS. These cells were then pulsed with 250 nM $pHlicKer^{RE}$ for 15 min and chased for 30 min, washed with 1× PBS three times and then imaged in HBSS using a widefield microscope.

Electrophysiology. Kv11.1 current ($I_{Kv11.1}$) was measured by the whole-cell patch-clamp technique as described previously[17,53]. The standard extracellular saline bath solution contained (in mmol/L) 137 NaCl, 4 KCl, 1.8 $CaCl_2$, 1 $MgCl_2$, 10 glucose, and 10 HEPES (pH 7.4 with NaOH). The modified extracellular saline bath solution to mimic the ionic conditions in recycling endosomes contained in (mmol/L) 90 NaCl, 30 KCl, 0.05 $CaCl_2$, 1 $MgCl_2$, 10 glucose, and 10 MES (pH 6.5 with NaOH). The intracellular pipette solution contained (in mmol/L) 130 KCl, 1 $MgCl_2$, 5 EGTA, 5 MgATP, and 10 HEPES (pH 7.2 with KOH). An Axopatch-200B patch clamp amplifier (Molecular Devices) was used to record membrane currents and measure capacitance. The uncompensated pipette resistance was 1-3 MΩ and series resistance was compensated between 75 and 85%. After obtaining intracellular access, only cells with membrane seal resistances >1 GΩ were used. The holding potential in experiments was −80 mV in recordings done in standard extracellular bath or −100 mV in recordings done in the modified extracellular saline bath. In the standard extracellular saline bath, peak $I_{Kv11.1}$ was measured at a test-pulse of −50 mV

for 5 s immediately following depolarizing pre-pulse voltage steps from −80 to 70 mV in 10 -mV increments for 5 s. In the modified extracellular saline bath, peak $I_{Kv11.1}$ was measured at a test-pulse of −100 mV for 5 s immediately following depolarizing pre-pulse voltage steps from −80 to 70 mV in 10 -mV increments for 5 s. The voltage steps were applied every 20 s. Data are reported as $I_{Kv11.1}$ density (peak $I_{Kv11.1}$ normalized in each cell to its cell capacitance). Individual cell data were fit by the Boltzmann function[17,53] to calculate the maximal current density (I_{MAX}), the midpoint potential for $I_{Kv11.1}$ activation (V½), and slope factor, k, as defined by the mV/*e-fold* change in $I_{Kv11.1}$. All voltage-clamp experiments were performed at 22 °C to 23 °C within 1 to 2 hours after cells were removed from their culture conditions. Voltage protocols and data analysis were done with pCLAMP 11.0 (Molecular Devices) and Graphpad (Prism) computer software.

Extended Data

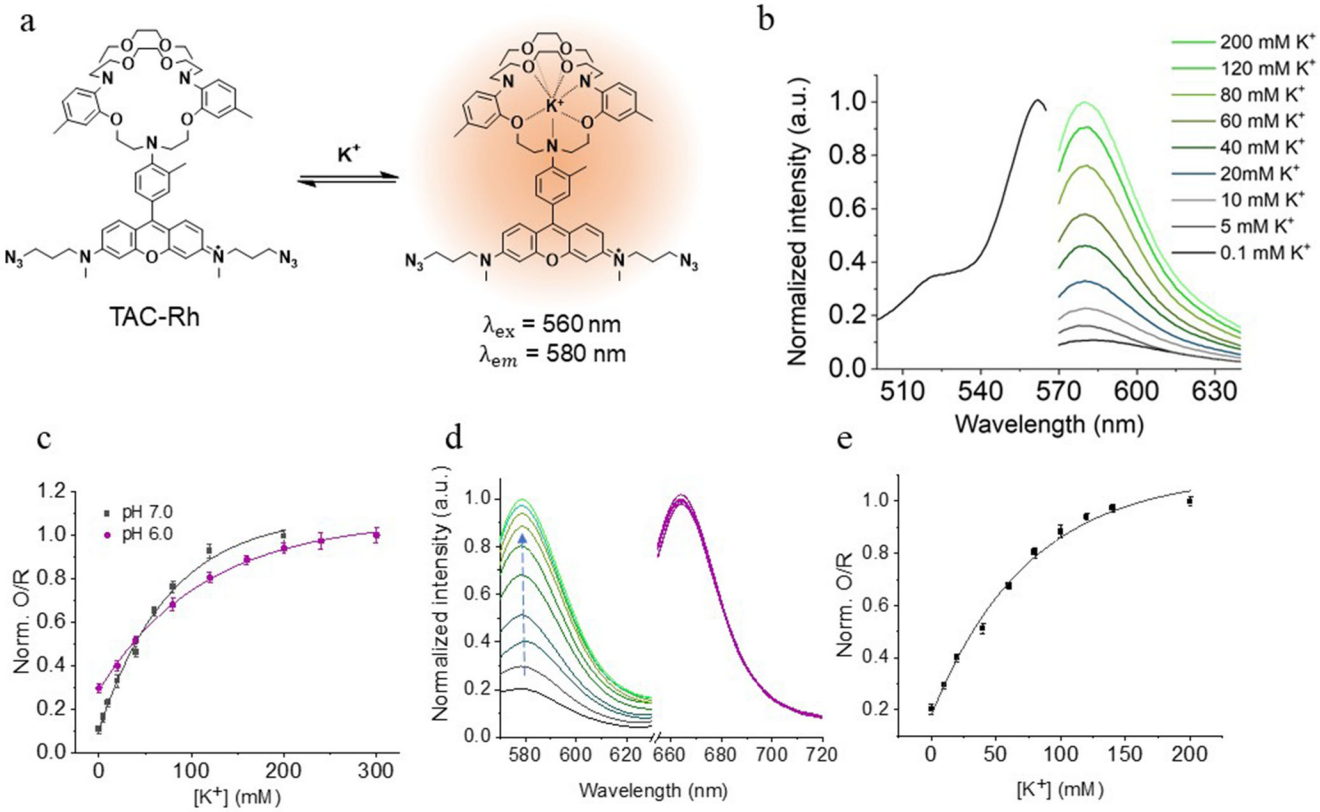

Extended Data Fig 1 |. TAC-Rh fluorescence response is a function of both pH and K^+.
a, Working principle of K^+ sensing by TAC-Rh. **b**, Excitation (black) and emission (green) spectra of TAC-Rh. Emission intensity increased with increasing K^+ concentration at pH = 7.0. **c**, Normalized O/R ratio of TAC-Rh/Alexa Fluor 647 with increasing [K^+] at pH 7.0 and 6.0. Error bar represents mean + s.e.m. of three independent experiments. **d**, Fluorescence emission spectra of *pHlicKer*^{RE} corresponding to TAC-Rh (green) and Alexa Fluor 647 (red) with increasing [K^+] at pH = 7.0. **e**, Normalized O/R ratio of TAC-Rh/Alexa Fluor 647

with increasing [K^+] at pH 7.0 Error bar represents mean + s.e.m. of three independent experiments.

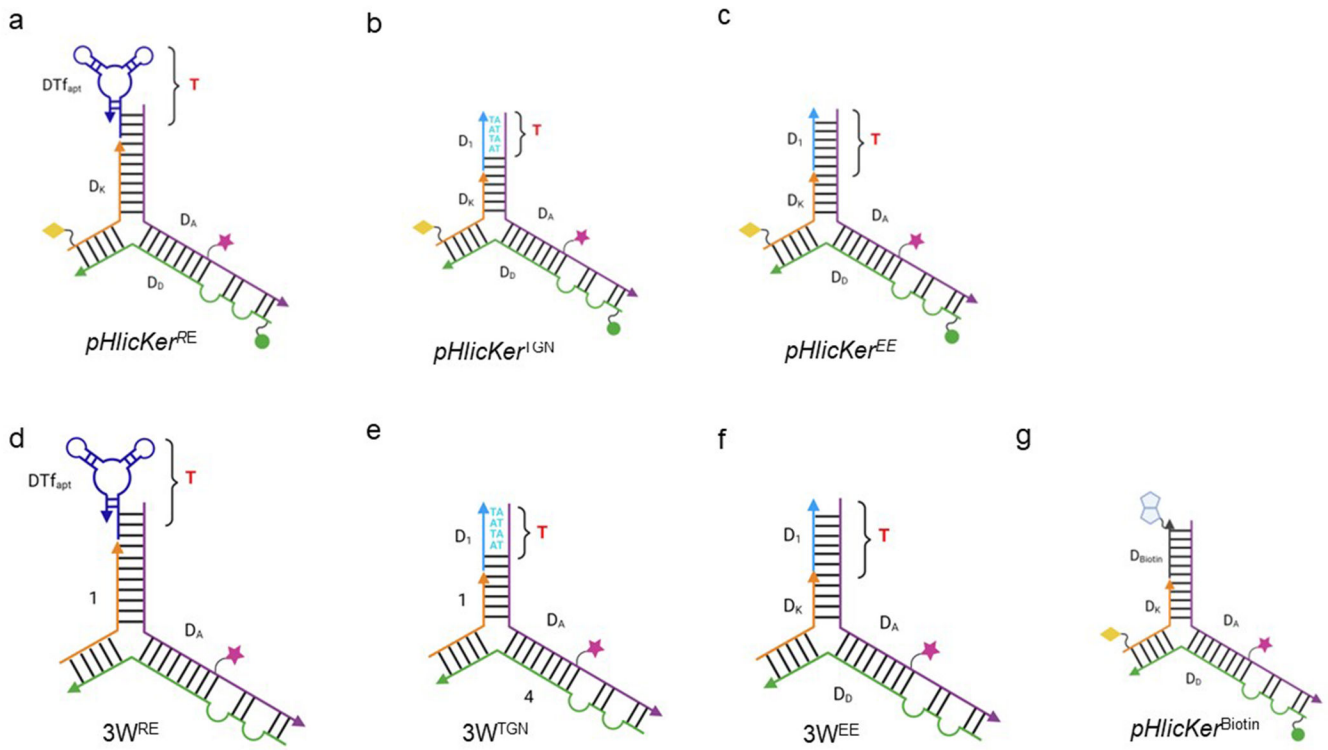

Extended Data Fig 2 |.

Targeting modules (T) in organelle-specific *pHlicKer* variants. **a**, *pHlicKer*^{RE} localizes in recycling endosomes (REs) by transferrin receptor (TfR) mediated endocytosis. T is an aptamer that binds TfR. **b**, *pHlicKer*^{TGN} is retrogradely trafficked by an scFv-furin chimera to the trans Golgi network (TGN). T is a $d(AT)_4$ sequence (cyan) in *pHlicKer* that sequence-specifically binds a single chain variable fragment (scFv) fused to the extracellular domain of furin. **c**, *pHlicKer*^{EE} localizes in early endosomes (EEs) by scavenger receptor mediated endocytosis. T is a duplex DNA domain, which is an excellent ligand for scavenger receptors. **d-f**, Three way (3W) junctions $3W^{RE}$, $3W^{TGN}$ and $3W^{EE}$ are made from the same sequences as *pHlicKer*^{RE}, *pHlicKer*^{TGN} and *pHlicKer*^{EE} and lack the Alexa488 and TAC-Rh fluorophores for colocalization studies with fluorescent markers of the RE, TGN and EE. **g**, *pHlicKer*^{Biotin} incorporates a biotin (grey pentagons) as indicated for immobilization on streptavidin coated beads.

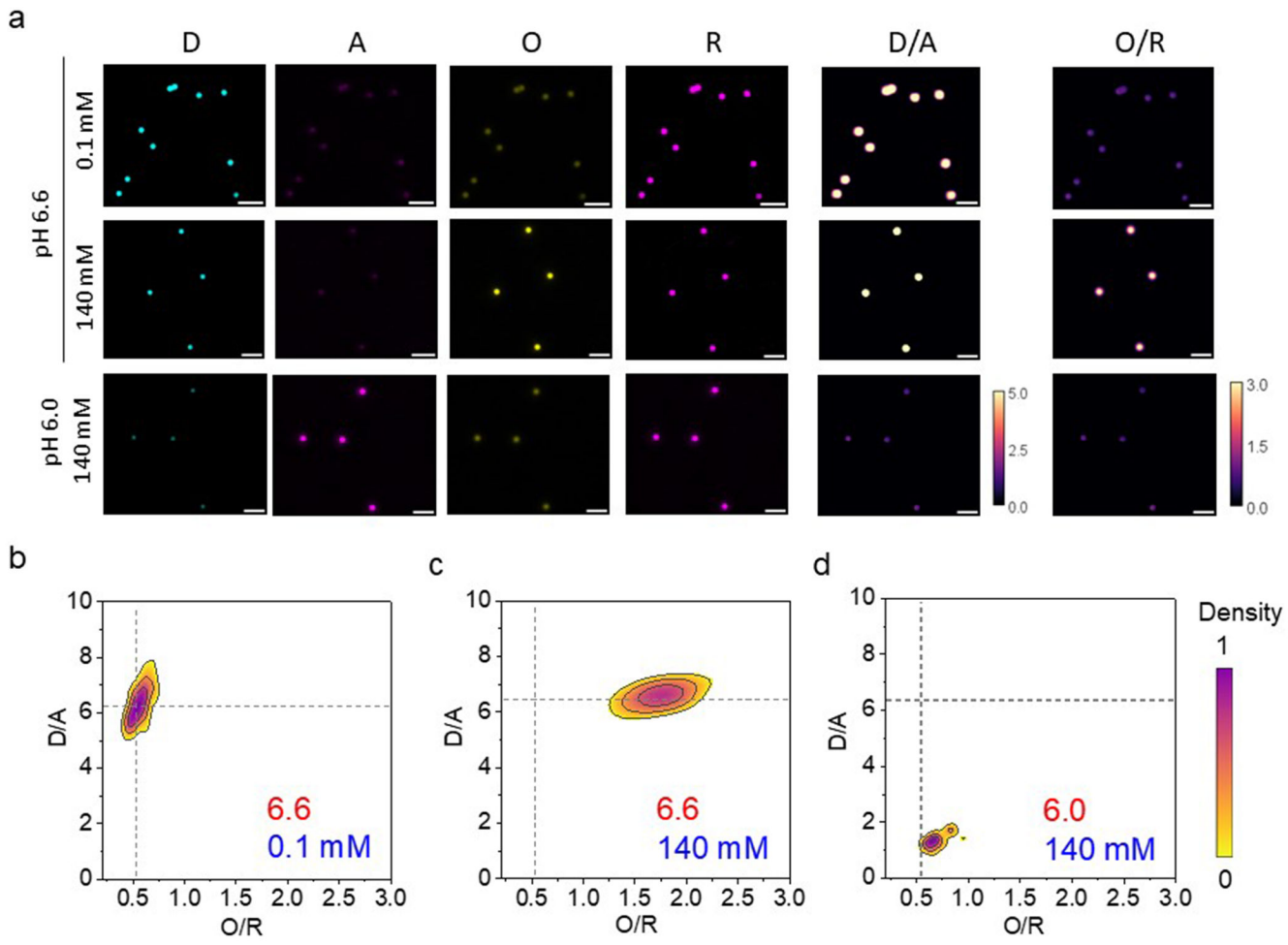

Extended Data Fig 3 |. Calibration of *pHlicKer* on beads.

a, Representative images of *pHlicKer*^{Biotin} on beads clamped at indicated pH and K^+ levels, imaged in the donor channel (D), acceptor channel (A), TMR (O), and Alexa Fluor 647 (R) channels. D/A and O/R are the corresponding pixel-wise pseudocolor images. (n = 100 beads). Scale bars, 5 μm. **b-d,** 2-IM profiles of beads clamped at indicated pH and [K^+]. Experiments were performed in triplicate (n = 100 beads).

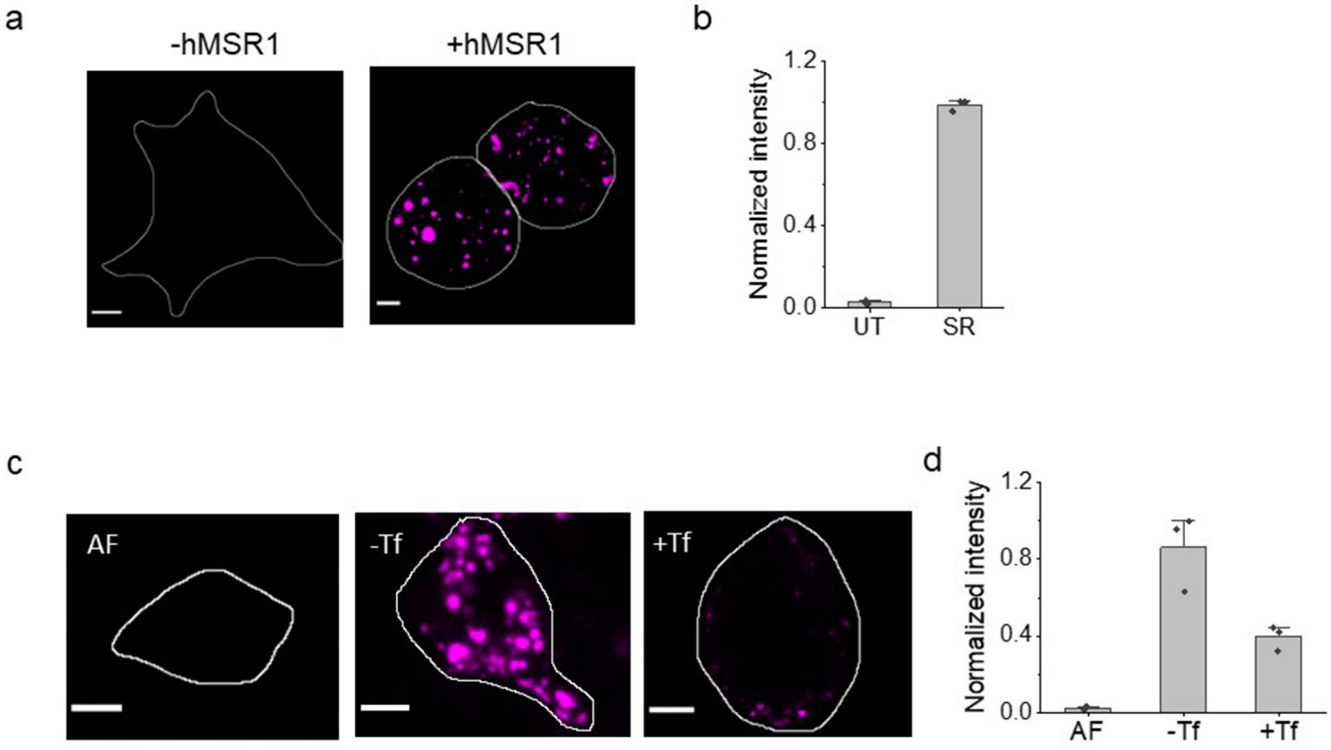

Extended Data Fig 4 |. Targetability of $3W^{EE}$ and $3W^{RE}$.

a, Uptake by HEK 293T cells expressing human scavenger receptor (hMSR1). Representative images of the uptake of Alexa 647 labelled $3W^{EE}$ in untransfected and hMSR1 transfected HEK 293T cells. Scale bars, 5 μm. **b,** Normalized whole cell intensities for (**a**). Data represent mean ± s.e.m (n=15 cells). hMSR1 expressing HEK 293T cells showed effective internalization of *pHlicKer*^{EE}, revealing uptake is by scavenger receptors. **c,** Competition experiments with $3W^{RE}$ and excess unlabelled transferrin (Tf) in HEK 293T cells. Representative fluorescence images of HEK 293T cells pulsed with $3W^{RE}$ (500 nM) in the presence (+Tf, 20 μM) and absence (-Tf) of Tf. Cells are imaged in the Alexa 647 channel. AF, autofluorescence. Scale bars, 5 μm. **d,** Normalized intensities for (**c**). Data represent mean ± s.e.m (n=15 cells). *pHlicKer*^{RE} internalization by HEK 293T cell is competed out by excess Tf, revealing that uptake is mediated by transferrin receptor mediated endocytosis.

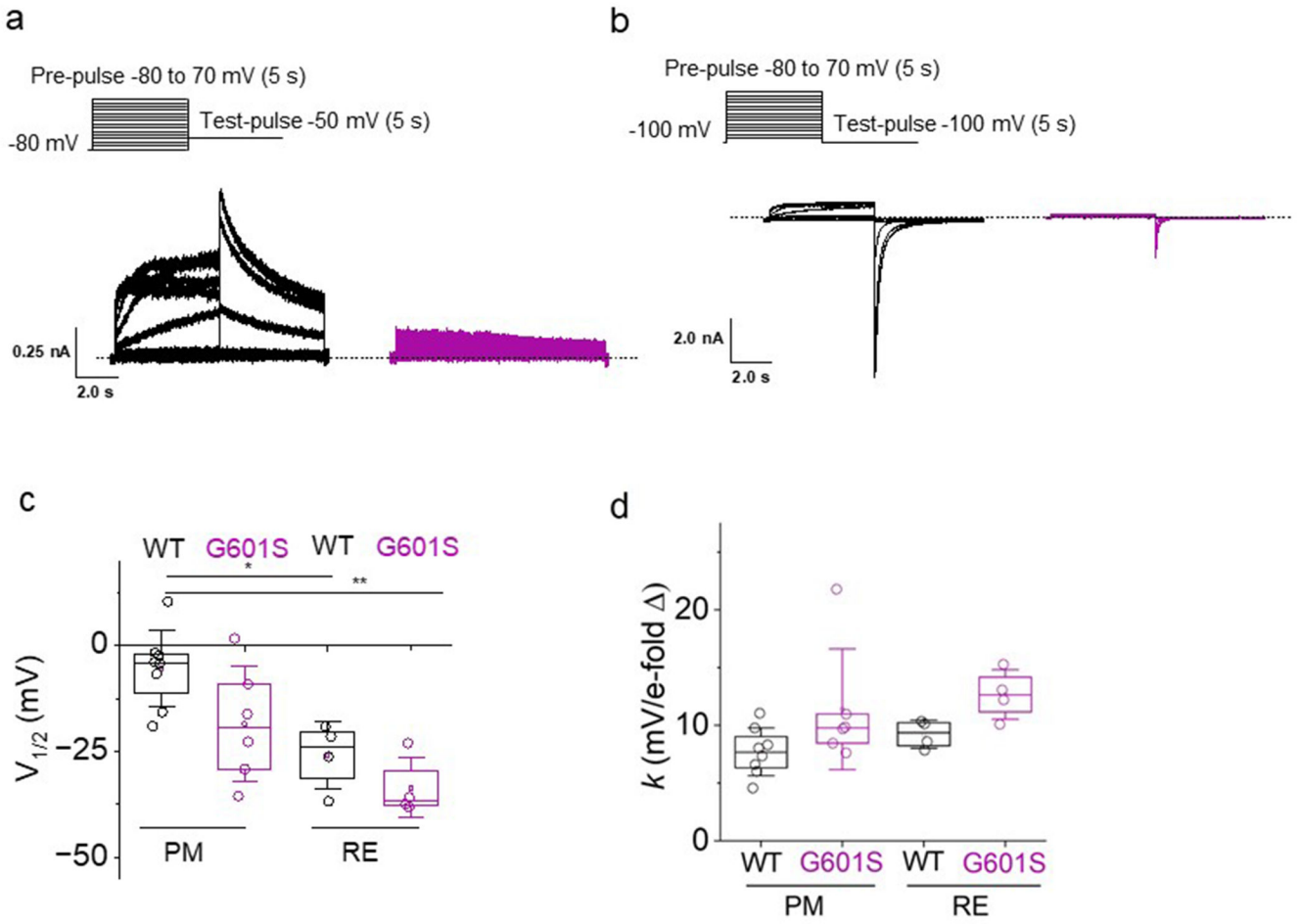

Extended Data Fig 5 |. Kv11.1 channel activity in transmembrane ion gradients equivalent to plasma membrane and recycling endosome.

a, b, Representative families of currents measured from cells stably expressing WT-Kv11.1 (black) or G601S- Kv11.1 (magenta) channel proteins using the voltage protocol shown in inset. **a,** Traces recorded using the standard extracellular saline or **b**, the modified extracellular saline to mimic recycling endosomes. Individual I-V relations were generated for each cell in each condition by plotting the peak current recorded during the test-pulse as a function of the pre-pulse (Figure 6i–j). The individual I-V relations were described using a Boltzmann equation to calculate the I_{MAX} (Figure 6i–j), **c**, midpoint potential for $I_{Kv11.1}$ activation ($V_{1/2}$), or **d,** the slope factor for $I_{Kv11.1}$ current activation (*k*).

Supplementary Material

Refer to Web version on PubMed Central for supplementary material.

Acknowledgements

We thank Eduardo Perozo and Ai Lin Chun for valuable comments on the manuscript. We thank the integrated light microscopy facilities at the University of Chicago. Y.K. acknowledges funding from NIH grants DP1GM149751, 1R01NS112139-01A1, R21HL161825-01A1, 1R01GM147197-01 FA9550-19-0003 from the AFOSR, HFSP grant no: RGP0032/2022, and the Ono Pharma Foundation.

Data availability

All data related to the study are included in the article and supporting information. The raw data supporting Figures 1–6, Extended data Figures, Supplementary Figures respectively, are available for public access at Figshare[54–61].

https://figshare.com/articles/dataset/Figure_1/23713359

https://figshare.com/articles/dataset/Figure_2/23713554

https://figshare.com/articles/dataset/Figure_3/23713776

https://figshare.com/articles/dataset/Figure_4/23713821

https://figshare.com/articles/dataset/Figure_5/23713833

https://figshare.com/articles/dataset/Figure_6/23713851

https://figshare.com/articles/dataset/Extended_data_figures/23713899

https://figshare.com/articles/dataset/Supplementary_Figures/23713947

References

1. Foo B, Williamson B, Young JC, Lukacs G & Shrier A hERG quality control and the long QT syndrome. J Physiol (Lond) 594, 2469–2481 (2016). [PubMed: 26718903]
2. Saminathan A et al. A DNA-based voltmeter for organelles. Nat. Nanotechnol 16, 96–103 (2021). [PubMed: 33139937]
3. Irannejad R et al. Conformational biosensors reveal GPCR signalling from endosomes. Nature 495, 534–538 (2013). [PubMed: 23515162]
4. Tao X, Avalos JL, Chen J & MacKinnon R Crystal structure of the eukaryotic strong inward-rectifier K+ channel Kir2.2 at 3.1 A resolution. Science 326, 1668–1674 (2009). [PubMed: 20019282]
5. Sambath K et al. Potassium ion fluorescence probes: structures, properties and bioimaging. ChemPhotoChem 5, 317–325 (2021).
6. He H, Mortellaro MA, Leiner MJP, Fraatz RJ & Tusa JK A fluorescent sensor with high selectivity and sensitivity for potassium in water. J. Am. Chem. Soc 125, 1468–1469 (2003). [PubMed: 12568593]
7. Padmawar P, Yao X, Bloch O, Manley GT & Verkman AS K+ waves in brain cortex visualized using a long-wavelength K+-sensing fluorescent indicator. Nat. Methods 2, 825–827 (2005). [PubMed: 16278651]
8. Schapiro FB & Grinstein S Determinants of the pH of the Golgi complex. J. Biol. Chem 275, 21025–21032 (2000). [PubMed: 10748071]
9. Reeves EP et al. Killing activity of neutrophils is mediated through activation of proteases by K+ flux. Nature 416, 291–297 (2002). [PubMed: 11907569]
10. Chakraborty K, Veetil AT, Jaffrey SR & Krishnan Y Nucleic Acid-Based Nanodevices in Biological Imaging. Annu. Rev. Biochem 85, 349–373 (2016). [PubMed: 27294440]
11. Saminathan A, Zajac M, Anees P & Krishnan Y Organelle-level precision with next-generation targeting technologies. Nat. Rev. Mater (2021) doi:10.1038/s41578-021-00396-8.
12. Krishnan Y, Zou J & Jani MS Quantitative imaging of biochemistry in situ and at the nanoscale. ACS Cent. Sci 6, 1938–1954 (2020). [PubMed: 33274271]
13. Modi S et al. A DNA nanomachine that maps spatial and temporal pH changes inside living cells. Nat. Nanotechnol 4, 325–330 (2009). [PubMed: 19421220]

14. Modi S, Nizak C, Surana S, Halder S & Krishnan Y Two DNA nanomachines map pH changes along intersecting endocytic pathways inside the same cell. Nat. Nanotechnol 8, 459–467 (2013). [PubMed: 23708428]
15. Narayanaswamy N et al. A pH-correctable, DNA-based fluorescent reporter for organellar calcium. Nat. Methods 16, 95–102 (2019). [PubMed: 30532082]
16. Saha S, Prakash V, Halder S, Chakraborty K & Krishnan Y A pH-independent DNA nanodevice for quantifying chloride transport in organelles of living cells. Nat. Nanotechnol 10, 645–651 (2015). [PubMed: 26098226]
17. Zhou Z et al. Properties of HERG channels stably expressed in HEK 293 cells studied at physiological temperature. Biophys. J 74, 230–241 (1998). [PubMed: 9449325]
18. Surana S, Shenoy AR & Krishnan Y Designing DNA nanodevices for compatibility with the immune system of higher organisms. Nat. Nanotechnol 10, 741–747 (2015). [PubMed: 26329110]
19. Surana S, Bhat JM, Koushika SP & Krishnan Y An autonomous DNA nanomachine maps spatiotemporal pH changes in a multicellular living organism. Nat. Commun 2, 340 (2011). [PubMed: 21654640]
20. Bhatia D, Surana S, Chakraborty S, Koushika SP & Krishnan Y A synthetic icosahedral DNA-based host-cargo complex for functional in vivo imaging. Nat. Commun 2, 339 (2011). [PubMed: 21654639]
21. Veetil AT et al. Cell-targetable DNA nanocapsules for spatiotemporal release of caged bioactive small molecules. Nat. Nanotechnol 12, 1183–1189 (2017). [PubMed: 28825714]
22. Leung K, Chakraborty K, Saminathan A & Krishnan Y A DNA nanomachine chemically resolves lysosomes in live cells. Nat. Nanotechnol 14, 176–183 (2019). [PubMed: 30510277]
23. Jani MS, Zou J, Veetil AT & Krishnan Y A DNA-based fluorescent probe maps NOS3 activity with subcellular spatial resolution. Nat. Chem. Biol 16, 660–666 (2020). [PubMed: 32152543]
24. Osei-Owusu J et al. Proton-activated chloride channel PAC regulates endosomal acidification and transferrin receptor-mediated endocytosis. Cell Rep. 34, 108683 (2021). [PubMed: 33503418]
25. Di A et al. The TWIK2 Potassium Efflux Channel in Macrophages Mediates NLRP3 Inflammasome-Induced Inflammation. Immunity 49, 56–65.e4 (2018). [PubMed: 29958799]
26. Huang LS et al. Endosomal trafficking of two pore K+ efflux channel TWIK2 to plasmalemma mediates NLRP3 inflammasome activation and inflammatory injury. eLife 12, (2023).
27. Sanguinetti MC, Jiang C, Curran ME & Keating MT A mechanistic link between an inherited and an acquired cardiac arrhythmia: HERG encodes the IKr potassium channel. Cell 81, 299–307 (1995). [PubMed: 7736582]
28. Keating MT & Sanguinetti MC Molecular and cellular mechanisms of cardiac arrhythmias. Cell 104, 569–580 (2001). [PubMed: 11239413]
29. Sanguinetti MC & Tristani-Firouzi M hERG potassium channels and cardiac arrhythmia. Nature 440, 463–469 (2006). [PubMed: 16554806]
30. Zhou Z, Gong Q & January CT Correction of defective protein trafficking of a mutant HERG potassium channel in human long QT syndrome. Pharmacological and temperature effects. J. Biol. Chem 274, 31123–31126 (1999). [PubMed: 10531299]
31. Anderson CL et al. Large-scale mutational analysis of Kv11.1 reveals molecular insights into type 2 long QT syndrome. Nat. Commun 5, 5535 (2014). [PubMed: 25417810]
32. Maxfield FR & McGraw TE Endocytic recycling. Nat. Rev. Mol. Cell Biol 5, 121–132 (2004). [PubMed: 15040445]
33. Hardel N, Harmel N, Zolles G, Fakler B & Klöcker N Recycling endosomes supply cardiac pacemaker channels for regulated surface expression. Cardiovasc. Res 79, 52–60 (2008). [PubMed: 18326556]
34. Mohammad S, Zhou Z, Gong Q & January CT Blockage of the HERG human cardiac K+ channel by the gastrointestinal prokinetic agent cisapride. Am. J. Physiol 273, H2534–8 (1997). [PubMed: 9374794]
35. Nakamura N, Tanaka S, Teko Y, Mitsui K & Kanazawa H Four Na+/H+ exchanger isoforms are distributed to Golgi and post-Golgi compartments and are involved in organelle pH regulation. J. Biol. Chem 280, 1561–1572 (2005). [PubMed: 15522866]

36. Kellokumpu S Golgi ph, ion and redox homeostasis: how much do they really matter? Front. Cell Dev. Biol 7, 93 (2019). [PubMed: 31263697]
37. Solé L & Tamkun MM Trafficking mechanisms underlying Nav channel subcellular localization in neurons. Channels (Austin) 14, 1–17 (2020).
38. Smith JL et al. Pharmacological correction of long QT-linked mutations in KCNH2 (hERG) increases the trafficking of Kv11.1 channels stored in the transitional endoplasmic reticulum. Am J Physiol, Cell Physiol 305, C919–30 (2013). [PubMed: 23864605]
39. Ficker E, Obejero-Paz CA, Zhao S & Brown AM The binding site for channel blockers that rescue misprocessed human long QT syndrome type 2 ether-a-gogo-related gene (HERG) mutations. J. Biol. Chem 277, 4989–4998 (2002). [PubMed: 11741928]
40. Qile M et al. LUF7244 plus Dofetilide Rescues Aberrant Kv11.1 Trafficking and Produces Functional IKv11.1. Mol. Pharmacol 97, 355–364 (2020). [PubMed: 32241959]
41. Bischof H et al. Novel genetically encoded fluorescent probes enable real-time detection of potassium in vitro and in vivo. Nat. Commun 8, 1422 (2017). [PubMed: 29127288]
42. Bezanilla F The voltage sensor in voltage-dependent ion channels. Physiol. Rev 80, 555–592 (2000). [PubMed: 10747201]
43. Bian J, Cui J & McDonald TV HERG K(+) channel activity is regulated by changes in phosphatidyl inositol 4,5-bisphosphate. Circ. Res 89, 1168–1176 (2001). [PubMed: 11739282]
44. Rodriguez N et al. Phosphatidylinositol-4,5-bisphosphate (PIP(2)) stabilizes the open pore conformation of the Kv11.1 (hERG) channel. Biophys. J 99, 1110–1118 (2010). [PubMed: 20712994]
45. Tan X, Thapa N, Choi S & Anderson RA Emerging roles of PtdIns(4,5)P2--beyond the plasma membrane. J. Cell Sci 128, 4047–4056 (2015). [PubMed: 26574506]
46. Zhang X, Hu M, Yang Y & Xu H Organellar TRP channels. Nat. Struct. Mol. Biol 25, 1009–1018 (2018). [PubMed: 30374082]
47. Xu H, Martinoia E & Szabo I Organellar channels and transporters. Cell Calcium 58, 1–10 (2015). [PubMed: 25795199]
48. Prakash V et al. Quantitative mapping of endosomal DNA processing by single molecule counting. Angew. Chem. Int. Ed 58, 3073–3076 (2019).
49. Delisle BP et al. Thapsigargin selectively rescues the trafficking defective LQT2 channels G601S and F805C. J. Biol. Chem 278, 35749–35754 (2003). [PubMed: 12837749]
50. Magadán JG, Barbieri MA, Mesa R, Stahl PD & Mayorga LS Rab22a regulates the sorting of transferrin to recycling endosomes. Mol. Cell. Biol 26, 2595–2614 (2006). [PubMed: 16537905]
51. van Galen J et al. Sphingomyelin homeostasis is required to form functional enzymatic domains at the trans-Golgi network. J. Cell Biol 206, 609–618 (2014). [PubMed: 25179630]
52. Modi S, Halder S, Nizak C & Krishnan Y Recombinant antibody mediated delivery of organelle-specific DNA pH sensors along endocytic pathways. Nanoscale 6, 1144–1152 (2014). [PubMed: 24297098]
53. Delisle BP et al. Intragenic suppression of trafficking-defective KCNH2 channels associated with long QT syndrome. Mol. Pharmacol 68, 233–240 (2005). [PubMed: 15851652]
54. Anees P et al. Detecting organelle-specific activity of potassium channels with a DNA nanodevice. Figure 1. 3D surface plots and selectivity studies. Figshare (2023) doi:10.6084/m9.figshare.23713359.v1.
55. Anees P et al. Detecting organelle-specific activity of potassium channels with a DNA nanodevice. Figure 2. 2-IM plots. Figshare (2023) doi:10.6084/m9.figshare.23713554.v1.
56. Anees P et al. Detecting organelle-specific activity of potassium channels with a DNA nanodevice. Figure 3. Colocalization data and 2-IM plots. Figshare (2023) doi:10.6084/m9.figshare.23713776.v1.
57. Anees P et al. Detecting organelle-specific activity of potassium channels with a DNA nanodevice. Figure 4. Colocalization data and 2-IM plots. Figshare (2023) doi:10.6084/m9.figshare.23713821.v1.
58. Anees P et al. Detecting organelle-specific activity of potassium channels with a DNA nanodevice. Figure 5. 2-IM plots. Figshare (2023) doi:10.6084/m9.figshare.23713833.v1.

59. Anees P et al. Detecting organelle-specific activity of potassium channels with a DNA nanodevice. Figure 6. 2-IM plots, I-V curves and peak current density plots. Figshare (2023) doi:10.6084/m9.figshare.23713851.v1.

60. Anees P et al. Detecting organelle-specific activity of potassium channels with a DNA nanodevice. Extended data figures. fluorescence spectra, 2-IM plots, competition experiments, standard current-voltage (I-V) relationships. Figshare (2023) doi:10.6084/m9.figshare.23713899.v1.

61. Anees P et al. Detecting organelle-specific activity of potassium channels with a DNA nanodevice. Supplementary Figures. fluorescence spectra, absorption spectra, 2-IM plots, colocalization data, blind test. Figshare (2023) doi:10.6084/m9.figshare.23713947.v1.

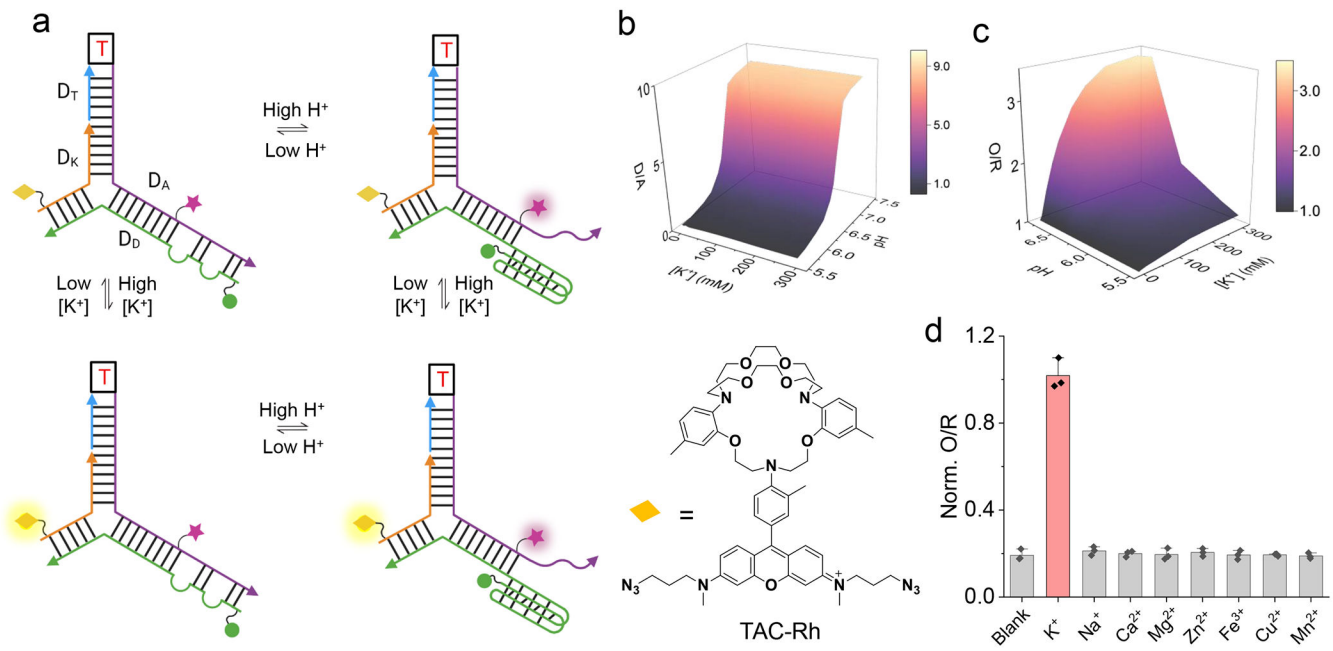

Fig. 1 |. *pHlicKer* is a selective, combination reporter for pH and K^+.

a, Working principle of *pHlicKer*. D_K, D_D and D_A represent three DNA strands that display a targeting module, T, on *pHlicKer*. pH-induced FRET between Alexa Fluor 488 (donor; green sphere) and Alexa Fluor 647 (acceptor; magenta star) reports on pH ratiometrically. K^+-sensitive dye, TAC-Rh (yellow diamond; λ_{ex} = 560 nm), and Alexa Fluor 647 (λ_{ex} = 650 nm) report K^+ ratiometrically by direct excitation. **b-c**, 3D surface plot of D/A, the pH response (**b**), and O/R, the K^+ response (**c**), of *pHlicKer*^{Biotin} immobilized on beads as a function of pH and [K^+]. The pH response of *pHlicKer* is insensitive to K^+, but its K^+ response is sensitive to acidic pH. **d**, Normalized O/R values of *pHlicKer*^{Biotin} in response to other biologically relevant cations show *pHlicKer* is specific to K^+. Concentrations were: K^+ and Na^+ (150 mM); Ca^{2+} and Mg^{2+} (1.5 mM); Zn^{2+}, Fe^{3+}, Cu^{2+} and Mn^{2+} (100 μM). Error bars represent standard error of mean (s.e.m.) from three independent experiments.

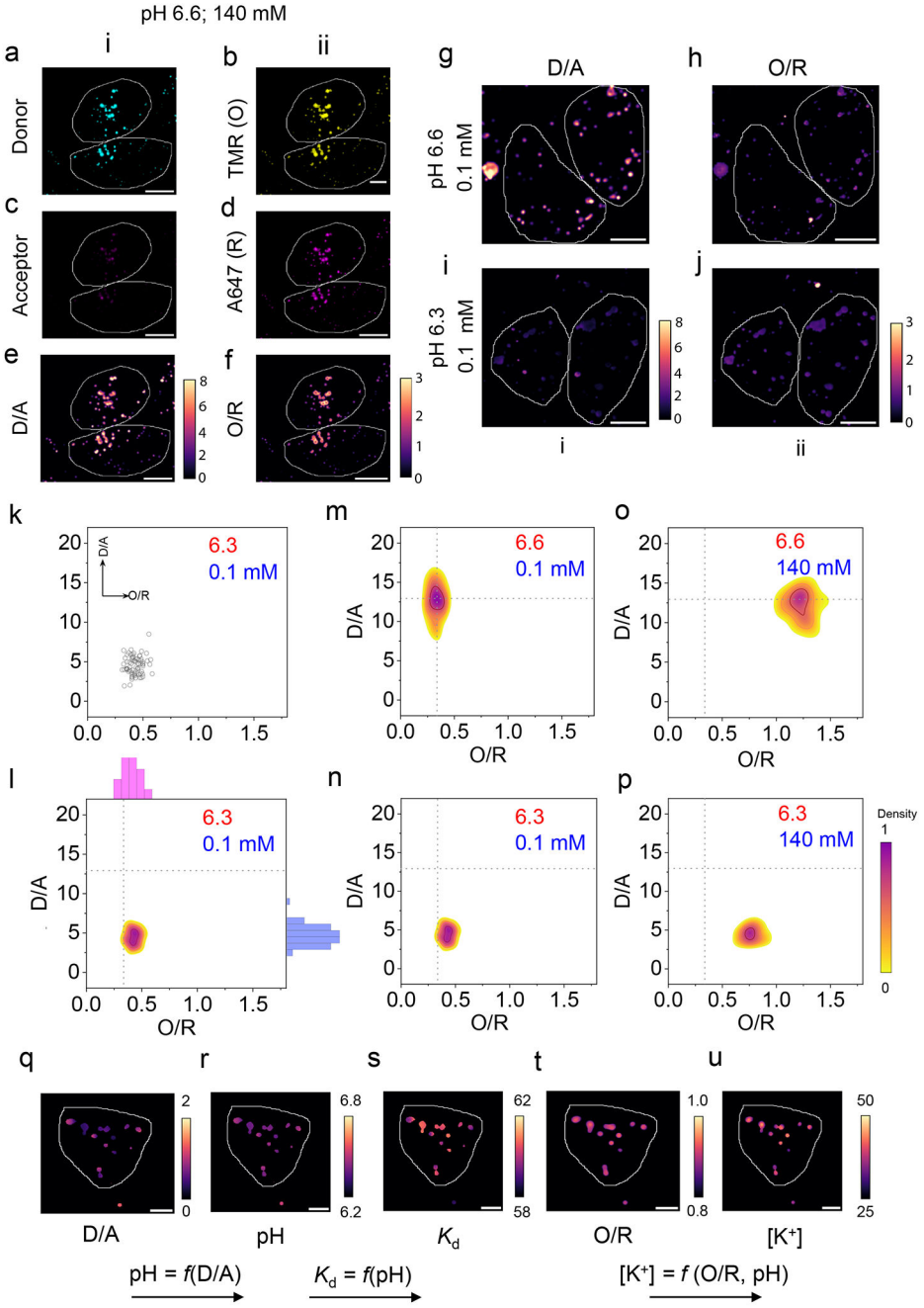

Fig. 2 |. Intracellular calibration of *pHlicKer*.

a-d, Representative *pHlicKer*^{RE} -labeled RE of HEK 293T cells imaged in the donor (D), TAC-Rh (TMR, O), acceptor (A), and Alexa Fluor 647 (R) channels, clamped at pH 6.6 and 140 mM K^+. **e**, D/A and **f**, O/R are the corresponding pixel-wise pseudocolor images. **g-j**, Representative pseudo-coloured D/A and O/R maps of RE in HEK 293T cells clamped at the indicated pH and [K^+]. **k**, Scatter plot of D/A versus the R/G values of endosomes in HEK 293T cells clamped at the indicated pH and [K^+] (n = 14 cells, n = 76 endosomes). Each data point corresponds to a single endosome. **l**, Scatter plot in **k** represented as a

pseudocolored density plot, i.e, 2IM profile, and projected histograms. Purple and yellow correspond to populations with higher and lower frequencies of occurrence. **m-p**. 2-IM profiles of HEK 293T cells clamped at the indicated pH (red font) and [K^+] (blue font). Dotted lines are a frame of reference centered on the maximum in **l**. Experiments performed in triplicate (Fig 2m: (n = 17 cells, n = 75 endosomes; Fig 2o: (n = 16 cells, n = 83 endosomes; Fig 2p: (n = 15 cells, n = 60 endosomes). **q**-**u**, [K^+] maps are obtained by converting the (**q**) D/A map of *pHlicKer*^{RE}-labeled REs into (**r**) a pH map. (**r**) is converted into (**s**) a K_d map, where the pH value at each pixel is replaced by the value of K_d at that pH. The product of the (**t**) O/R map and K_d map yields (**u**) the [K^+] map. "$f(x)$" is function of x. Data are from one experiment representative of trial of three independent experiments. All scale bars, 5 μm.

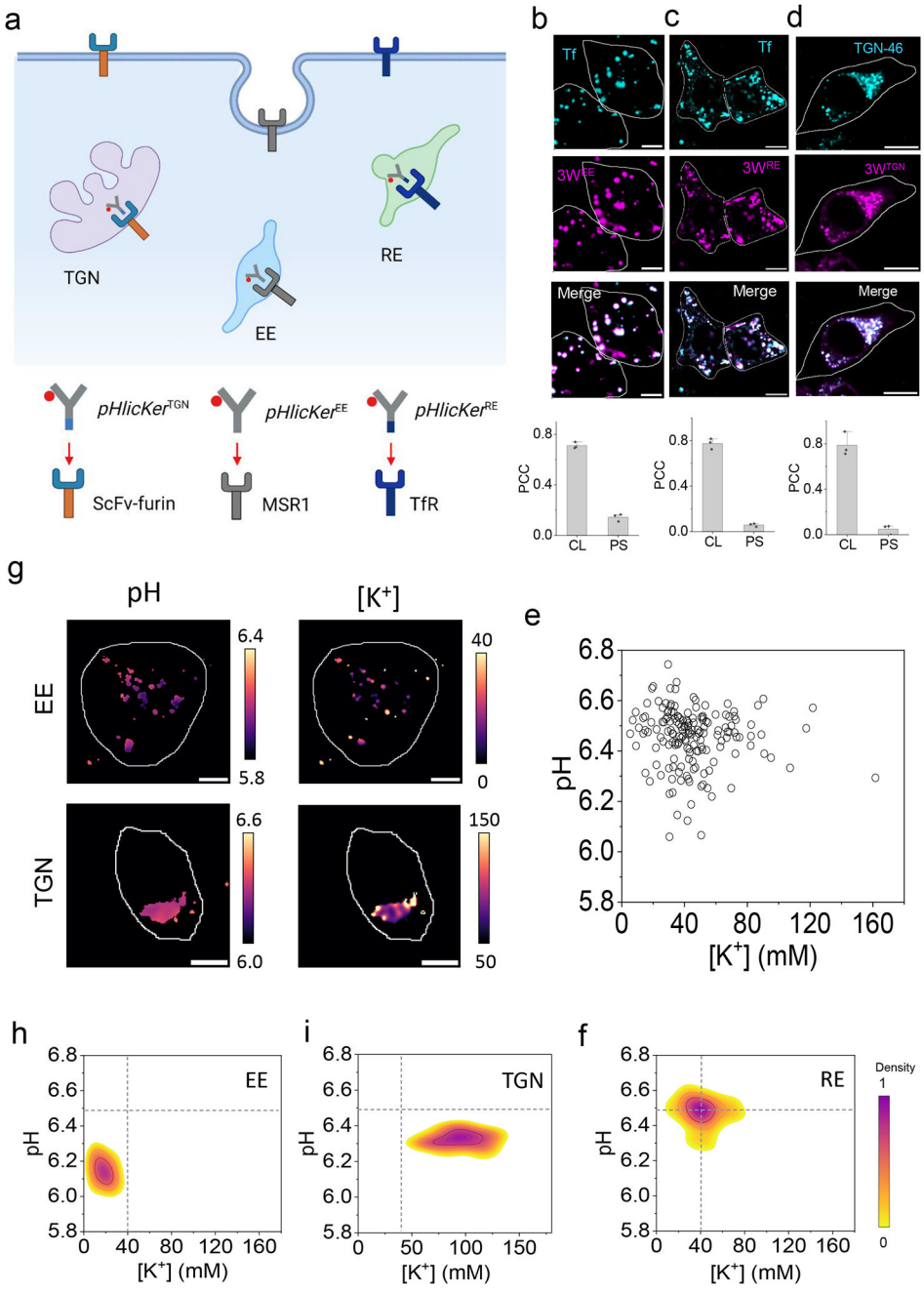

Fig. 3 |. pH and K^+ maps in endocytic organelles.

a, Schematic of organelle targeting: *pHlicKer*^{RE} targets REs via the transferrin receptor (TfR) mediated endocytosis, by displaying a TfR aptamer. *pHlicKer*^{EE} targets EEs via scavenger receptor (MSR1)-mediated endocytosis, by its dsDNA domains. *pHlicKer*^{TGN} targets the TGN via retrograde trafficking of furin, using a $d(AT)_4$ domain that binds an scFv domain fused to furin. Cells express each receptor endogenously or by transfection **b**, Colocalization of fluorescently labeled Tf (Tf-Alexa488, cyan) with EE labeled by $3W^{EE}$ (magenta) in hMSR1-transfected HEK 293T cells. **c**, Colocalization of RE tracer

(transferrin-Alexa488, cyan) and $3W^{RE}$ (magenta) in HEK 293T cells. **d**, Colocalization of TGN marker (TGN46-mCherry, cyan) and $3W^{TGN}$ (magenta) in scFv-furin-transfected HEK 293T cells. Scale bar, 5 μm. Pearson's correlation coefficient (PCC) of colocalization (CL) and pixel shift (PS) for **b-d**. Error bars represent mean ± s.e.m. of three independent trials for n = 15 cells. **e**, Representative scatter plots of pH versus $[K^+]$ of RE in HEK 293T cells. Each data point corresponds to a single endosome (n = 40 cells, n = 155 endosomes). **g**, Representative pseudocolor pH and $[K^+]$ maps of EE and TGN labeled with *pHlicKer*$^{EE/TGN}$. **f, h-i**, 2-IM profiles of pH and $[K^+]$ in RE, EE, and TGN. (Fig 3h: n = 15 cells, n = 65 endosomes; Fig 3i: n = 52 cells). Data represents one out of three independent experiments.

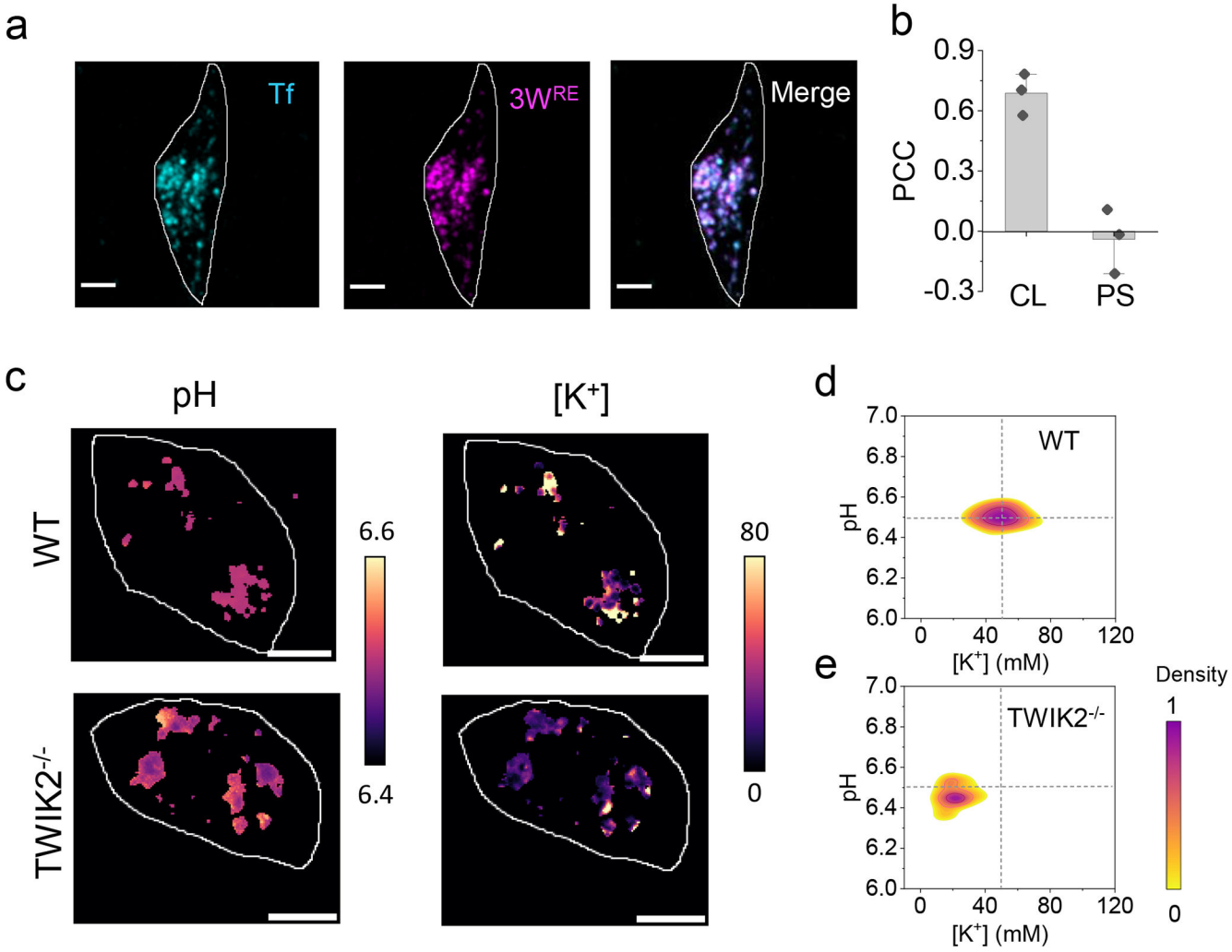

Fig. 4 |. pH and K^+ maps in RE of WT and TWIK2$^{-/-}$ BMDM cells.

a) Colocalization between RE tracer (transferrin-Alexa488, cyan) and 3W^{RE} (magenta) in BMDM cells. b) Pearson's correlation coefficient (PCC) of colocalization (CL) and pixel shift (PS) for a. Error bars represent mean ± s.e.m. of three independent trials for n = 16 cells. c) Representative pseudocolor pH and [K^+] maps of RE in WT and TWIK2$^{-/-}$ of BMDM cells labeled with *pHlicKer*^{RE}. d-e, 2-IM profiles of pH and [K^+] of RE in WT and TWIK2$^{-/-}$ of BMDM cells. (Fig 4d: n = 13 cells, n = 108 endosomes; Fig 4e: n = 13 cells, n = 106 endosomes). Data represents one out of three independent experiments.

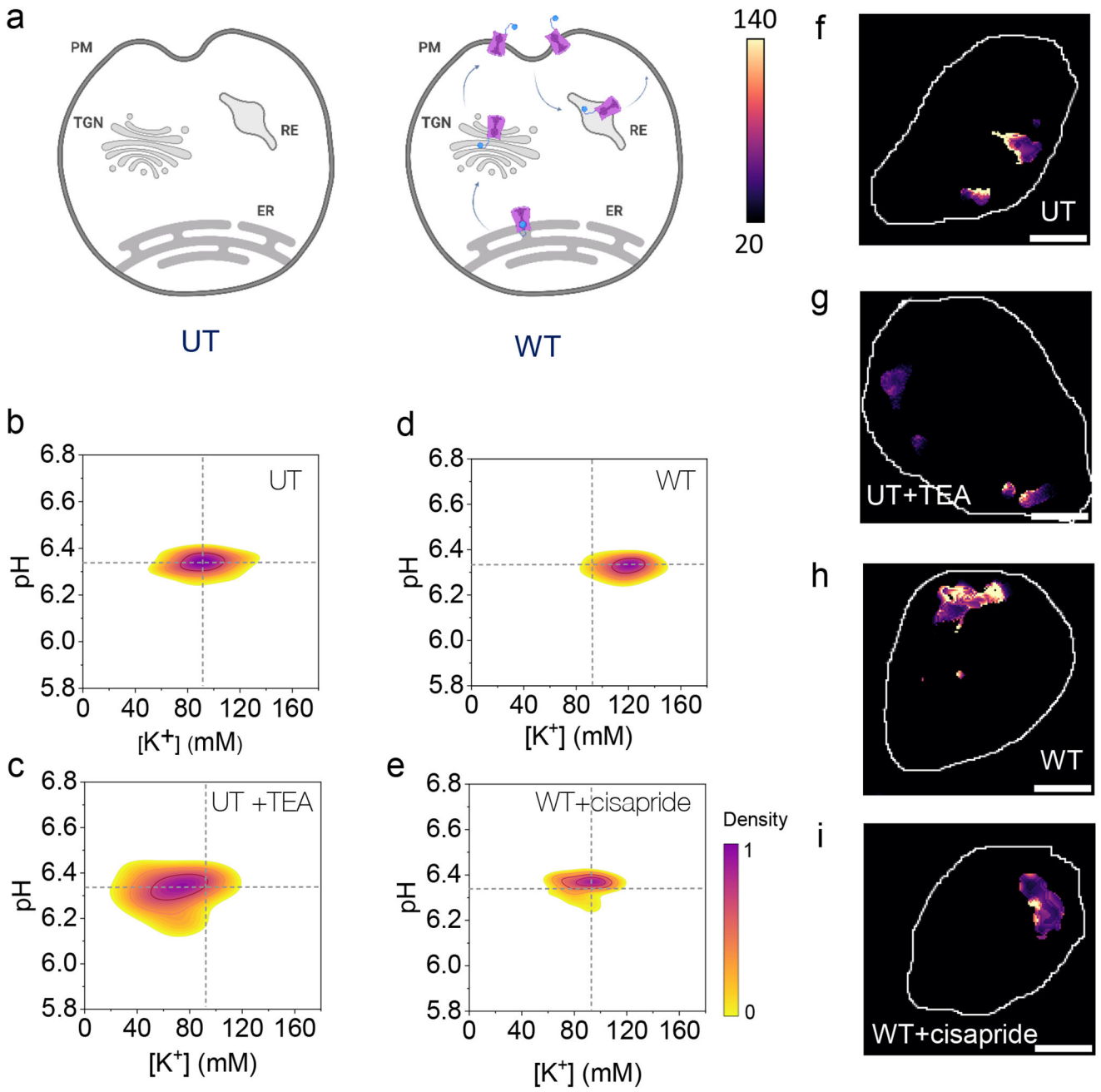

Fig. 5 |. *pHlicKer* reveals Kv11.1 channel activity in TGN.

a, Schematic of HEK 293T cells without endogenous Kv11.1 channels (UT) and stably expressing wild type Kv11.1 channels (WT). Kv11.1 channels traffic to the plasma membrane (PM) of WT cells via the TGN and are recycled via REs. **b-e**, $[K^+]_{TGN}$ and pH values in UT cells without (n = 38 cells) (**b**) and treated with tetraethyl ammonium chloride (TEA) (n = 39 cells) (**c**), WT cells without (n = 23 cells) (**d**) and treated with cisapride (n = 25 cells) (**e**). **f-i**, Representative pseudocolor $[K^+]$ maps of TGN labeled

with *pHlicKer*^{TGN} for the indicated conditions. Data are from one representative trial of independent experiments in triplicate (**b-e**).

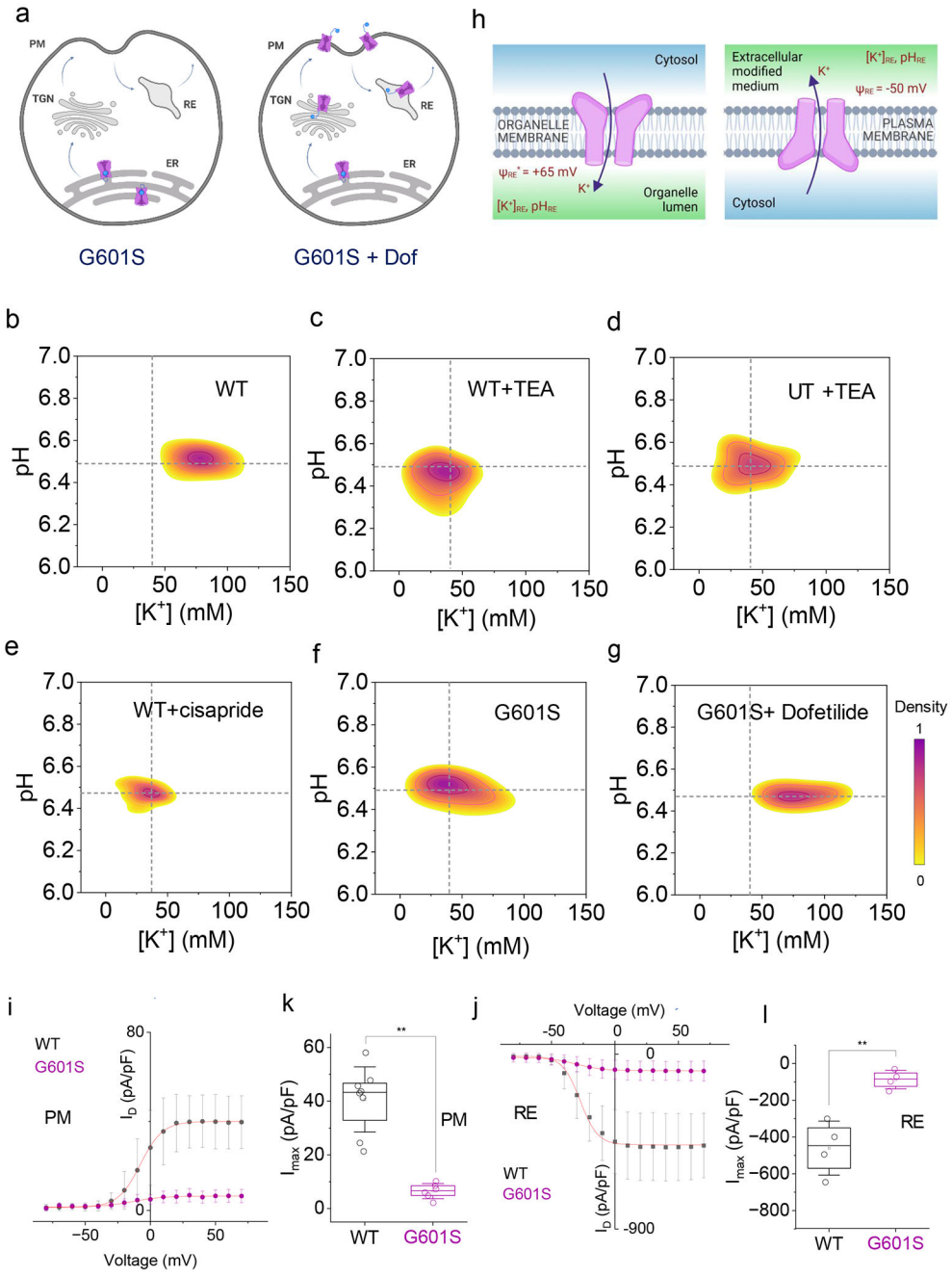

Fig. 6 |. *pHlicKer* probes channel activity, trafficking defects and rescue of trafficking.

a, Schematic of HEK 293T cells stably expressing Kv11.1 channels with a missense mutation (G601S) that cannot exit the endoplasmic reticulum (ER) unless cells are treated with dofetilide (Dof). **b-g**, $[K^+]_{RE}$ and pH values of recycling endosomes (REs) in WT cells without (n = 25 cells, n = 58 endosomes) (**b**) and treated with tetraethyl ammonium chloride (TEA) (n = 20 cells, n = 97 endosomes) (**c**), UT cells treated with TEA (n = 33 cells, n = 135 endosomes) (**d**), WT cells treated with cisapride (n = 26 cells, n = 98 endosomes) (**e**), G601S cells without (n = 21 cells, n = 64 endosomes) (**f**), treated with dofetilide overnight

and after wash out (n = 18 cells, n = 52 endosomes) (**g**). **h**, Modifying the composition of the extracellular medium mimics, at the plasma membrane, the conditions experienced by Kv11.1 channels in REs. **i-l**, I-V curves (**i**, **j**) and maximal $I_{Kv11.1}$ density (**k, l**) recorded from WT cells (black) and G601S cells (magenta) in standard extracellular saline (**i**, **k**) or modified extracellular saline mimicking ion gradients across RE membranes (**j**, **l**). $I_{Kv11.1}$ were recorded by pre-pulsing cells from −80 to 70 mV followed by a test-pulse to −50 mV (**i**) or −100 mV (**j**). Peak $I_{Kv11.1}$ measured during the test pulse as a function of the pre-pulse voltage to generate the I-V relations. Data are from one representative trial of independent experiments performed in triplicate (**b-g**), error bars represent standard deviations in **i-j**. (Fig 6i: n = 9 for WT and n = 6 for G601S; Fig 6j: n = 4 for WT and n = 4 for G601S). Embedded box plots indicate the 25th–75th percentile. Boxes and bars represent the s.e.m. and standard deviation, respectively. (Fig 6k, **p=0.001 and Fig 6l, **p=0.003) (one-way ANOVA with Tukey post hoc test). Ψ_{RE}* in panel h indicates membrane potential value considering the lumen to be positive.